tribology in industry

tribology in industry

⊤ contents ⊤

K.-D. BOUZAKIS

Announcment of "BalkanCoat" project, for interbalkan common research activities

During the " Contact' 95 " Conference, organized by the Society of the Bulgarian Tribologists and the Union of Mechanical Engineering in Sofia (31.10 - 02.11.1996), the president of the Balkan Tribological Association Prof. K.-D. Bouzakis of the Aristoteles University Thessaloniki, proposed the establishment of an interbalkan umbrella research project, in the area of development and applications of thin hard coatings. The aim of this project is to focus Balkan scientific and productive potential, on common research and development activities.

Advanced research on coating technology and its applications in cutting, in bearings, in improvment of material tribological characteristics etc., may offer an excellent challenge within a distinct framework of specific goals throughout the Balkan neighbourhood. This can be stated considering the excellent Balkan scientists research activities in the mentioned areas, results of which were presented in many high level papers, in the Second International Tribology Conference "Balkantrib 96" (June 1996) in Thessaloniki and included in the published proceedings of this Conference.

In order to exploit the previous by described encouraging situation an umbrella research project in the scientific field of coating technology and its applications, the "BalkanCoat" project was proposed by the president of the Balkan Tribological Association. The project has the ambition to enable the cooperation of interdisciplinary universities, associations, committees and research centres with the directly involved and interested manufacturing enterprises. A successful progress of this initiation shall lead to the realisation of various projects in different research fields under the "BalkanCoat" umbrella. The Balkan Tribological Association will be the project organising and guiding foundation, which will compose a joint of the separated research actions

A coordinator country per project will supervise and manage the research team. The first stage of each project is the development of high quality coatings by a Balkan coating producer. The quality of such coatings will be judged by tribological, indentation and fatigue tests, before their application in the final products, which can be specific parts of mature know how. Finally, these full scale products will be examined regarding their competence and ability to fulfil their development expectations. The Balkan products will be disseminated throughout the involved Balkan and European industry.

The budget of each project can be funded by national secretariats or ministries for research and technology of each involved country and the attentive manufacturing companies. An alternative funding possibility is to include distinct project parts in other relative European research projects such as the "Eureka" is. The president of the Balkan Tribological Association, who is national representative of Greece in "Eureka" shall provide his expertise in launching "BalkanCoat" projects into "Eureka". On that account, for each stage of the research action the corresponding partneres, in collaboration with the Balkan Tribological Association have to look for the necessary funding means to cover the project costs.

Interesting proposals under the umbrella of the "BalkanCoat" project can be submitted in the fields of coated conventional and hybrid bearings, of coated carbide cutting inserts etc.

For example, the goal of a related proposal could be the development of a new type of conventional or hybrid bearings (ceramic balls and steel rings) with coated races, in order to increase their rotational speed, to re-

duce the friction momentum and operating noise and to minimise the lubricant amount. This high demanding project requires low temperature coating deposition processes, to avoid the annealing of the races and extended quality tests, to prevent coating fatigue failure or increased wear. The quality tests will be separated in specimen examination (micro indentations, scratch tests, pin on disk tests, RCF tests e.tc) and experimental verification of the full scale product performance in special test rigs.

A further proposal of a research project under the " Balkan Coat " umbrella, could be the development of high quality coated ittserts. The Balkan and European market for this type of cutting tools is continuously growing regarding its magnitude and demands. The coating increase the tool performance and enhance the quality of the produced surfaces. Their fatigue or conventional wear must me checked with extended quality examinations, through fatigue reference tests and cutting experiments. In the frame of such a research project, parameters that have to be evaluated are the coating substrate combination, the friction, the wear performance, the heat generation and temperature behaviour, the workpiece surfaces etc.

The interested partners have to inform the coordinating committee, regarding their willness to participate to a "BalkanCoat" project, by sending a letter of intent, describing the works which they can conduct, as well as a short explanation about the project aims and the possible paricipants. For further information every interested partner, may contact the President of the Balkan Tribological Association, in the following address:

Prof. Dr.-Ing. habil. K. -D. Bouzakis
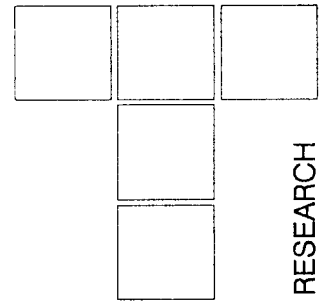*Laboratory for Machine tools and*
Machine Dynamics
Dept. of Mechanical Engineering
Aristoteles University of Thessaloniki
GR54006, Greece
Phone: (++3031) 996079, 996021
Fax: (++3031) 996059
E-mail:
Bouzakis@OLYMP.CCF.AUTH.GR

I. M. CIORNEI

Progresses of EHD Traction - Drivers

RESEARCH

The paper presents an analysis of friction power losses in elastohydrodynamic traction drives and underlines the possibilities of optimisation of these transmissions. Finally, several high performance traction drives are described.

Keywords: Friction, power losses, elastohydrodynamic, fluid

1. INTRODUCTION

Elastohydrodynamic traction drives represent one of the few fields in which the fluid friction is an useful phenomenon. Mechanical power is transmitted between the active elements of these drives by shear of elastohydrodynamic oil films. A part of the input power is dissipated in the film by parasitic shears. The remaining part represents the useful, transmitted power. In order to optimise the efficiency of elastohydrodynamic traction drives, the parasitic shears must be minimised. Traction drives conceived to this end are finally described in the paper.

2. FRICTION SOURCES IN ELASTOHYDRODYNAMIC TRACTION DRIVES

The fluid friction in EHD traction drives depends on many physical factors, of which the most important are macro and microgeometry of contacting elements, contact deformations as functions of material properties, lubricant nature and lubrication procedure, [1].

Nowadays it is convenient to measure global power losses in an EHD traction drive and to assess theoretically the components of friction. Consequently, the possibilities of optimisation of traction drives are severly limited, [1, 17, 19, 20]. As a general view, the power losses in a traction drive are composed of:

* friction in kinematic pairs;
* friction between moving elements and lubricating medium;
* friction in sealing elements;
* air ventilating for cooling the drive.

I. M. Ciornei
University of Suceava, 5800, Suceava, ROMANIA

As shown in figure 1, each of these components is a sum of several sources and can be identified finally as a part of global friction torque of the drive.

Losses by elastic hysteresis

During rolling, the inlet zone of the contact is subjected to loading, whereas the output is unloaded. The loading and unloading load-deformation curves do not concide and the area limited by them is a measure of the the energy loss by elastic hysteresis per cycle. This loss depends, [1, 2, 6, 18], on:

* elastic properties of contacting materials: as the material behaves more elastically, the energy losses decrease, whereas a viscous behaviour increases the power dissipation;
* contact stresses: at low levels of contact stresses the material behaves more linearly and the hysteress decreases;
* stressed volume.

Hysteresis losses are small in comparison to other losses. For instance, Drutowski [6], attributes a friction coefficient of 10^{-4} to hysteresis losses.

Althouth small, these losses increase as the transverse reduced radius of curvature of the raceways increases, as a result of increasing stressed volume.

Losses by nonuniform pressure distribution over the contact area

The hydrodynamic pressure generated in an EHD oil film yields a resultant force which is displaced towards the entry zone into the contact. It is assumed that this effect is responsible for the major part of rolling friction, [3].

Losses by microslip inside the contact

Two loaded active elements of a traction drive make contact over a finite area. Only a small fraction of the points placed in this area belong to the axoydes of mo-
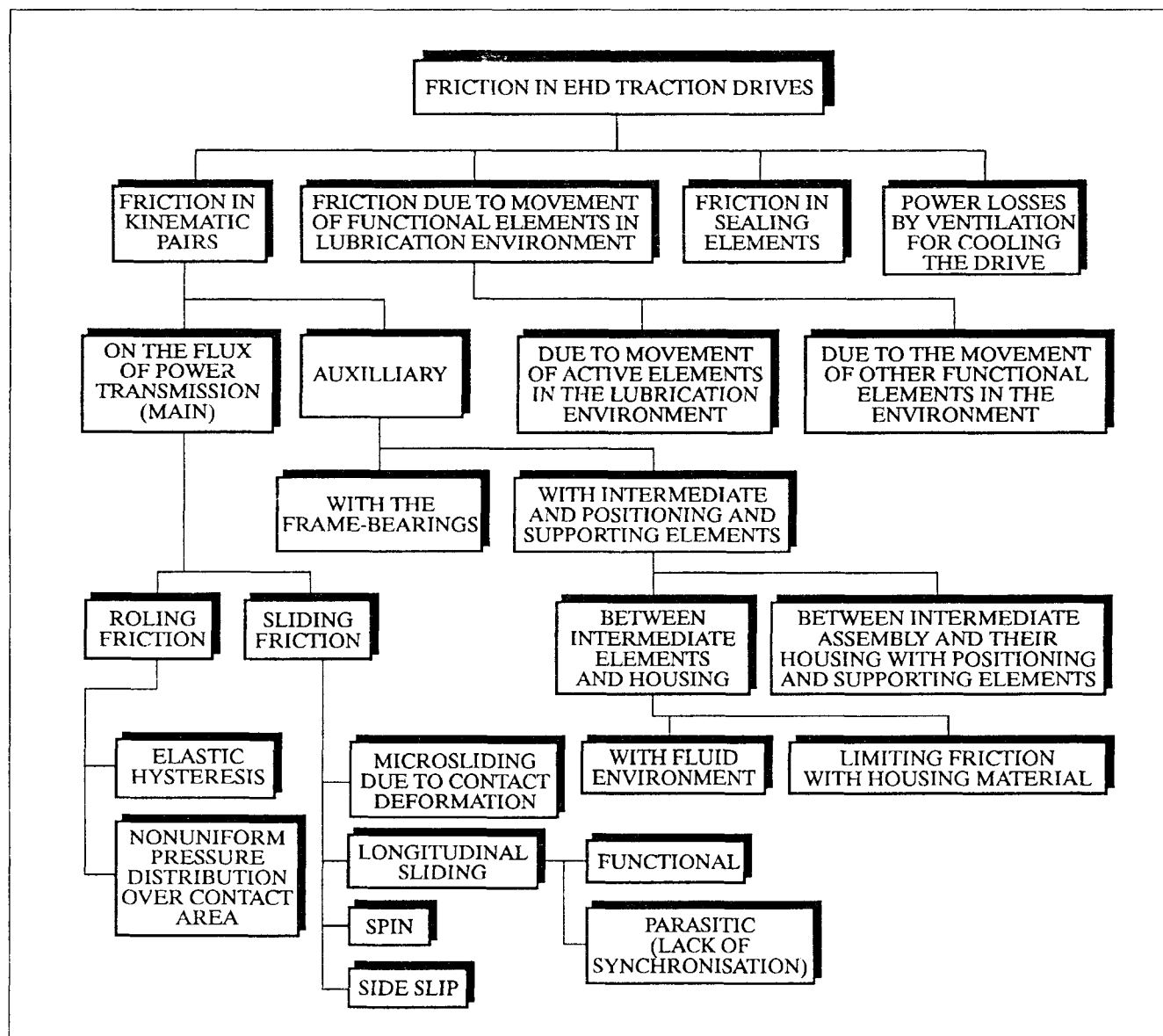
FRICTION IN EHD TRACTION DRIVES

- FRICTION IN KINEMATIC PAIRS
- FRICTION DUE TO MOVEMENT OF FUNCTIONAL ELEMENTS IN LUBRICATION ENVIRONMENT
- FRICTION IN SEALING ELEMENTS
- POWER LOSSES BY VENTILATION FOR COOLING THE DRIVE

- ON THE FLUX OF POWER TRANSMISSION (MAIN)
- AUXILLIARY
- DUE TO MOVEMENT OF ACTIVE ELEMENTS IN THE LUBRICATION ENVIRONMENT
- DUE TO THE MOVEMENT OF OTHER FUNCTIONAL ELEMENTS IN THE ENVIRONMENT

- WITH THE FRAME-BEARINGS
- WITH INTERMEDIATE AND POSITIONING AND SUPPORTING ELEMENTS

- ROLING FRICTION
- SLIDING FRICTION
- BETWEEN INTERMEDIATE ELEMENTS AND HOUSING
- BETWEEN INTERMEDIATE ASSEMBLY AND THEIR HOUSING WITH POSITIONING AND SUPPORTING ELEMENTS

- ELASTIC HYSTERESIS
- MICROSLIDING DUE TO CONTACT DEFORMATION
- WITH FLUID ENVIRONMENT
- LIMITING FRICTION WITH HOUSING MATERIAL

- NONUNIFORM PRESSURE DISTRIBUTION OVER CONTACT AREA
- LONGITUDINAL SLIDING
  - FUNCTIONAL
  - PARASITIC (LACK OF SYNCHRONISATION)
- SPIN
- SIDE SLIP

Figure1. Power disipation in EHD traction drives

tion. In the remaining points microslip occurs. This determines a local microshear of the oil film and consequently, shear stresses opposing the relative displacement. The resultant tangential force generates power dissipation, which increases with normal load and contact ellipticity, [8].

Losses by longitudinal sliding

Longitudinal sliding occurs in an EHD contact either as an useful result of the operating process or due to parasitic shear produced by lack of synchronisation between parallel intermediate elements. This sliding is the results of shear behaviour of the oil film and is characterised by the traction coefficient, [14]. Specific measures, such as the use of special lubricants, small rolling speeds or low temperatures are required to reduce the longitudinal sliding. Decrease of this sliding also requires a better synchronisation of multiple intermediate elements of the drive, [4], figure 2.
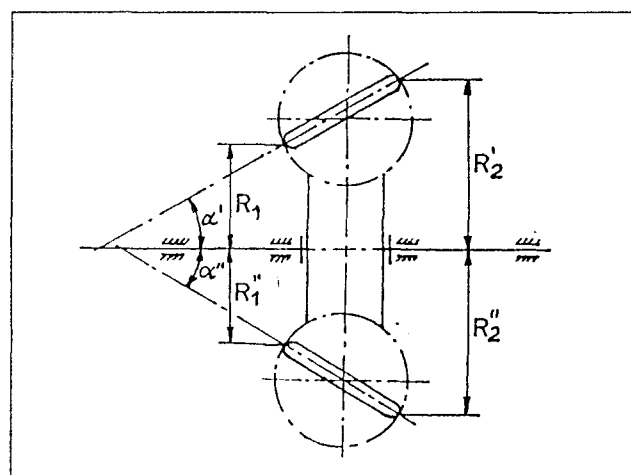

Figure 2. Lack of synchronisation between parallel intermediate elements

Losses by spin

The spin motion is a result of contact kinematics. Experimental and theoretical investigations, [1, 5, 7, 13, 15, 19], indicate that spin greatly affects traction curves.

Losses by side slip

Side slip occurs in a contact when the axes of the contacting elements are crossed. It reduces the traction capacity of the contact, as the spin does, [14].

Losses in main bearings

Usually, the rotating elements are supported in traction drives by rolling element bearings. These are heavily loaded by the normal load applier to the contact. As a result the friction in bearings is high and it dissipates an important part of the drive input power, [11].

Losses in auxilliary bearings

Friction pairs are formed between active elements and their housing. The sliding friction in these pairs can be high, especially when lubrication is poor. Auxilliary, ligthly loaded bearings are used to support and position the assembly of intermediate elements. The friction in these bearings is usually small.

Losses by churning become important when the surface of moving elements is large and the oil level is high. These can be reduced by using an incorporated pump to lubricate the drive and a low oil level.

Losses in sealing elements cannot be eliminated due to the design of the drives. Sealing elements having low power losses are therefore required. Losses by air ventilation occur because the drive case must be cooled by means of a fan placed on the input shaft. A low temperature is required by a correct opperation of drive.

Figure 3 indicates the values of the cross angle as function of maximum Hertz pressure which reduce the transmitting capacity of the contact by 10%o and 20%. It is advisable to keep this angle below 50'.

When thermal conductivity is predominant, the energy balance equation yields relationships for the ratio of

Figure 3. Limiting values for crossangle:
a) for 10% diminuation of transmitting capacity;
b) for 20% decrease of transmitting capacity;

traction force under spin and side slip to the traction force when no parasitic shears act, [10]. These can be written as:

$$\frac{F_{xparasite}}{F_x} = e^{-\alpha^* A S^{*2}} \; ; \quad A = \frac{\beta \cdot \eta_c \cdot u_2}{12 \cdot K_c}$$

where: $S^* = \omega_{sp} / \omega_j$, under spin and
$S^* = \Delta v / v$ under side slip.

In these relations β is the thermo-viscous coefficient, η_c the rolling speed and K_c the thermal conductivity.

Two possibilities exist to reduce the parasitic longitudinal sliding caused by lack of synchronisation between multiple intermediate elements of a traction drive. The first consists in rising the precision of the drive but it rises the price of the transmission. The second relies on supplementary mechanisms to allow the selfpositioning of the intermediate elements. It seems to be more efficient than the former.

As shown above, the friction in the bearings of the drive can be comparable to traction transmitted through the active contacts. As a result, if traction oils are unavailable, it is of utmost importance to unload the main bearings, [1].

The reduction of churning and ventilation losses requires lubrication of the drive by oil circulation. To this end a small incorporated oil pump can be used.

3. POSSIBILITES OF FRICTION DECREASE IN EHD TRACTION DRIVES

The major part of power losses in a traction drive is caused by rolling, longitudinal sliding, spin, side slip, churning and ventilation, [9]. The other power losses, shown in figure 1, are of the secondary importance.

The negative effect of spin upon power losses into an EHD contact is well known, [1, 5, 7, 9, 13, 15, 16]. It consists of a reduction of the slope of traction curves and of an increase of longitudinal sliding. This effect increases with rolling speed and it depends essentially on the rheological behaviour of the lubricant, [14]. The spin also reduces the maximum value of the traction coefficient, as shown in figure 4. At small values of spin-roll ratio this effect is unimportant, but it increases drastically above a limiting treshold of about (2-3)%, [1]. The influence of spin on maximum traction coefficient, at various rolling speeds, is shown in figure 5.

Relations to estimate the spin-roll ratio in a point contact, as deduced by authors, are given in Table 1. Some of these are experimentally verified, as seen in figures 6 and 7 for, respectively, a ball on disc and a kopp B traction drives.
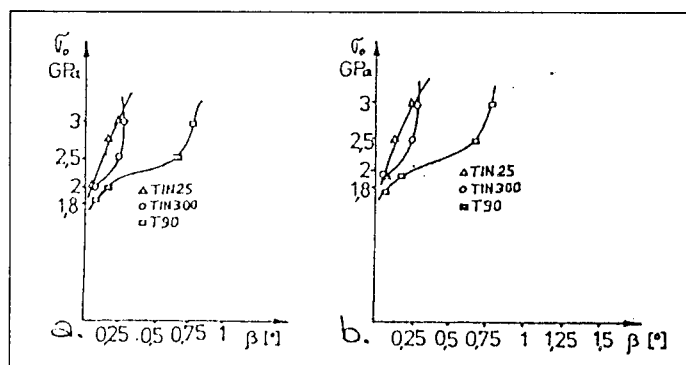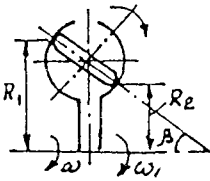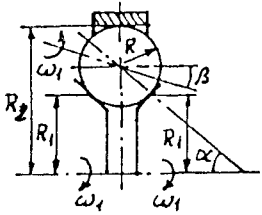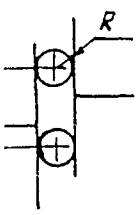
Table 1. Relations to estimate the spin-roll ration in a point contact

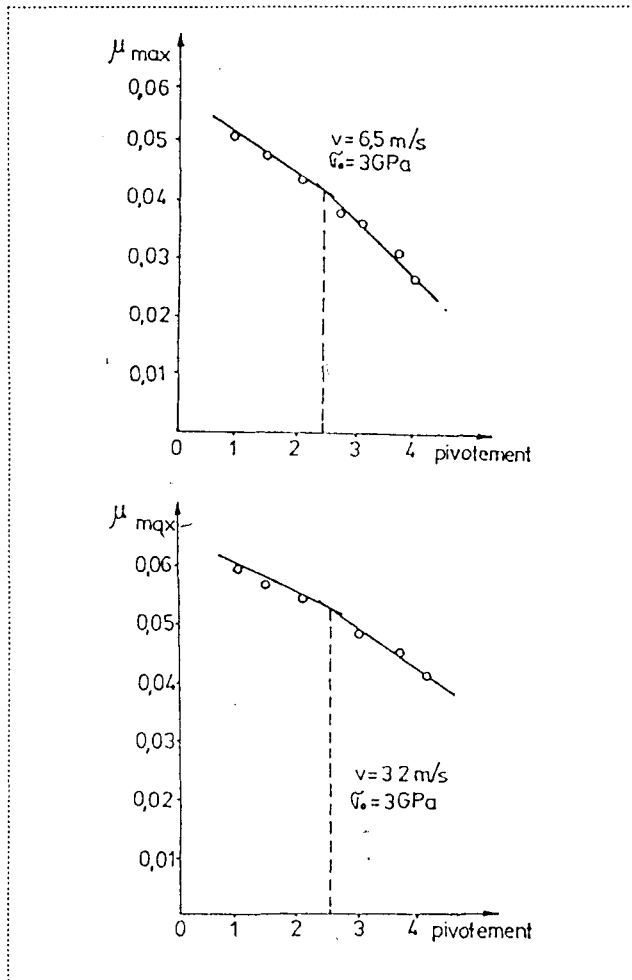| Nr. crt	1	2	3
Version / Diagrams	PERBURY	KOPP B	Ball on disc
Input contact	$\omega_{sp} = -\omega_1 \cos\beta$	$\omega_{sp} = \omega_1 \left[\sin\alpha + X \sin(\alpha - \beta) - \dfrac{\omega_1 R_1 SY \sin(\alpha - \beta)}{(1+\frac{S}{2})R\cos\alpha} \right]$ $X = \dfrac{(R_1 + R\cos\alpha)\sin\alpha - [R_1 tg(\alpha - \beta) + R\sin\alpha]\cos\alpha}{[R_1 tg(\alpha - \beta) + R\sin\alpha]\cos(\alpha - \beta) - (R_1 + R\cos\alpha)\sin(\alpha - \beta)}$ $Y = \dfrac{R\cos\alpha)[\sin\alpha - \cos\alpha\, tg(\alpha - \beta)]}{[R_1 tg(\alpha - \beta) + R\sin\alpha]\cos(\alpha - \beta) - (R_1 + R\cos\alpha)\sin(\alpha - \beta)}$	$\omega_{sp} = \dfrac{1}{2}(\omega_2 - \omega_1)\left(1 + \dfrac{R}{2r}\right)$
Output contact	$\omega_{sp} = \omega_1 \left\{ X\dfrac{R}{R_1}\cos\beta - \dfrac{S}{1+\frac{S}{2}}\left[X + \dfrac{SR_1}{(1+\frac{S}{2})R}\cdot\dfrac{2R}{R_1}\cos\beta \right] \right\}$	$\omega_{sp} = \omega_1 X[\sin(\alpha + \beta) - Y\sin\alpha] - \dfrac{R_1\omega_1 S_1}{(1+\frac{S}{2})R\cos\alpha}Y \cdot$ $\cdot[\sin(\alpha - \beta) - T^*\sin\alpha] + \dfrac{\omega_1 S\left[XR - \dfrac{R_1 S}{(1+\frac{S}{2})\cos\alpha}\right]}{(1+\frac{S}{2})R_1\cos\alpha\cos(\alpha + \beta)}$ $X^* = -\dfrac{R_1 + R\cos\alpha}{\sin\alpha - \cos\alpha\, tg(\alpha + \beta)}$ $Z^* = -\dfrac{R\sin\alpha + R_1 tg(\alpha + \beta)}{\sin\alpha - \cos\alpha\, tg(\alpha + \beta)}$	$\omega_{sp} = \dfrac{1}{2}(\omega_2 - \omega_1)\left(1 - \dfrac{R}{2r}\right)$
Observations	S-nondimensional longitudinal sliding	Contact ball-retaining ring $\omega_{sp} = -\omega_1 X \sin\beta - \dfrac{\omega_1 R_1 S}{(1+\frac{S}{2})R\cos\beta} Y \sin\beta$	

Figure 4. Effect of spin on maximum traction coefficient
for oil T90 EP2

Side slip occurs in a contact due to cross missalignment
of the element axes. The negative effect of this parasitic
shear is comparable to that of spin, [6]. High precision
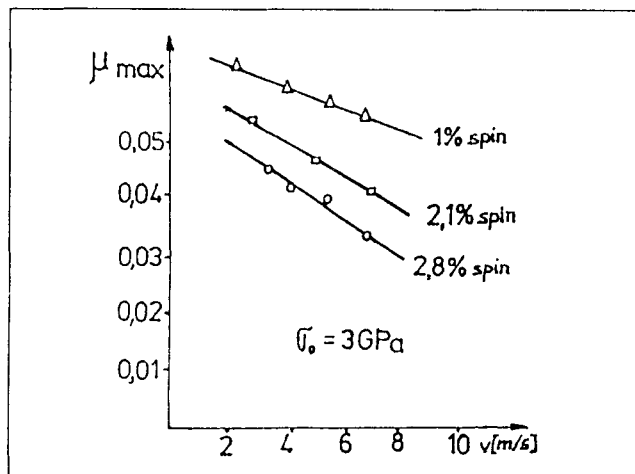machining and and mounting are required to reduce the
side slip.

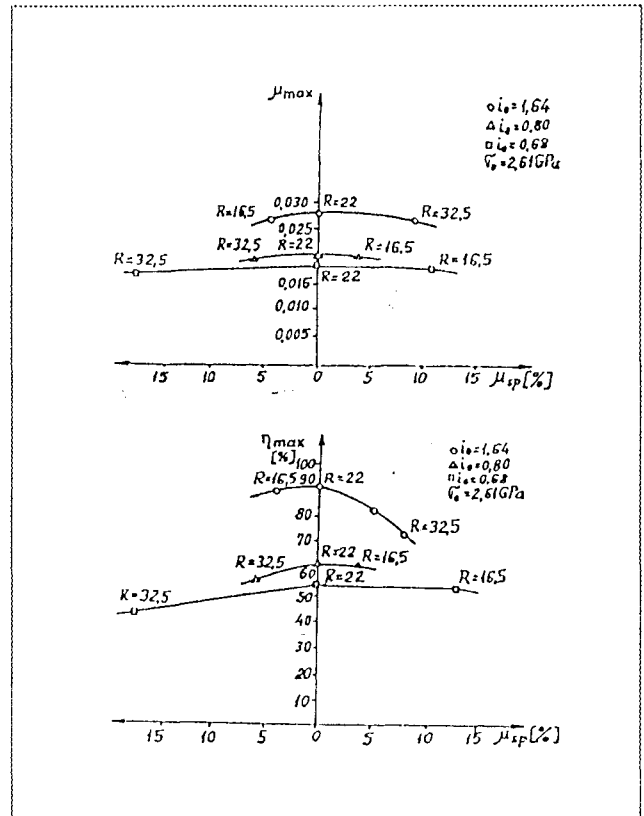Figure 5. Effect of rolling speed upon maximum
traction coefficient

Figure 6. Variation of maximum traction coeficient
and of efficiency with nondimensional
spin for ball on disc traction drive
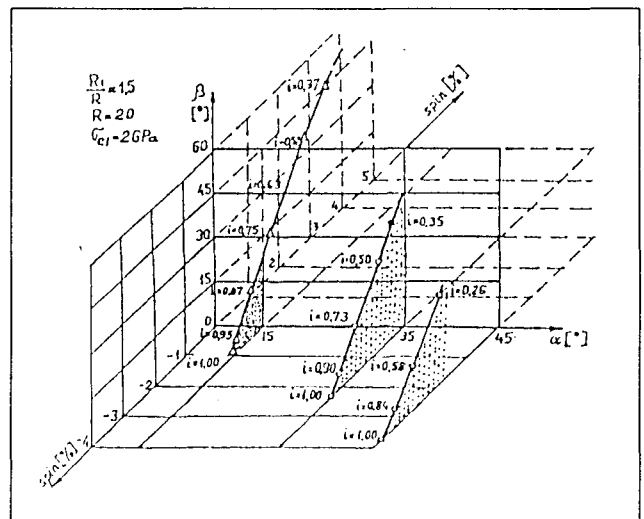
Figure 7. Spin in Kopp B traction drive

4. PROGRESS OF KOPP B TRACTION DRIVER RELATED TO AN OPTIMUM SPIN

The technical literature concerning traction drivers re-
commends finding solutions for spin reduction as a main
way of increasing the capable traction and efficiency.
Figures (8 - 11) show spin variation for different values
of the transmission ratio with respect to the contact
pressure and a series of structural dimensions, in the case
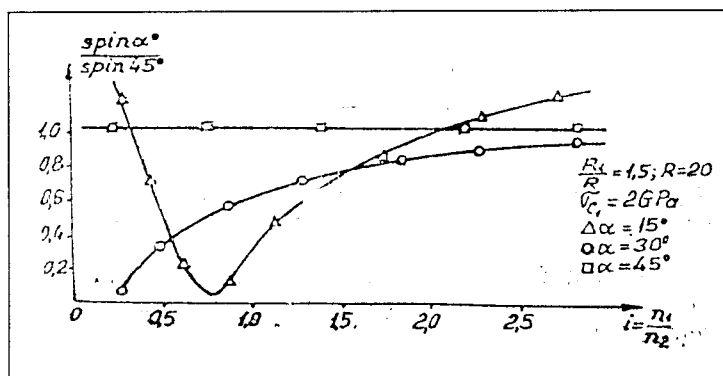of a Kopp B drives.

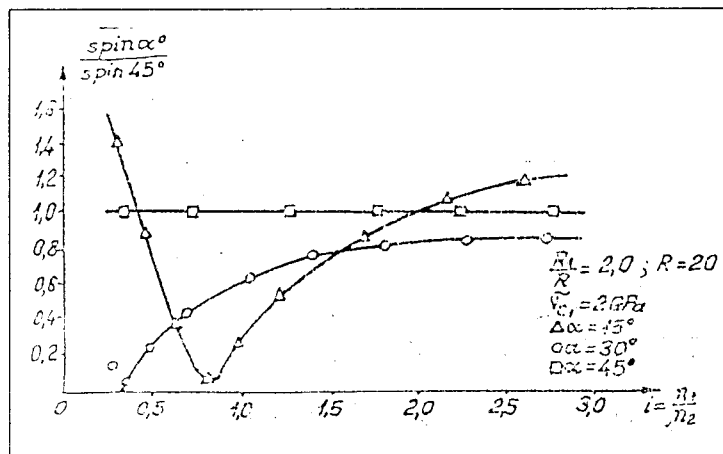Figure 8. Spin relative variation; contact inlet

Figure 9. Spin relative variation; contact inlet
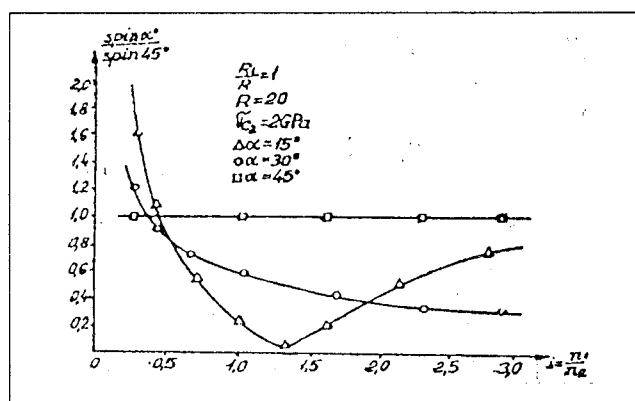

Figure 10. Spin relative variation; contact exit
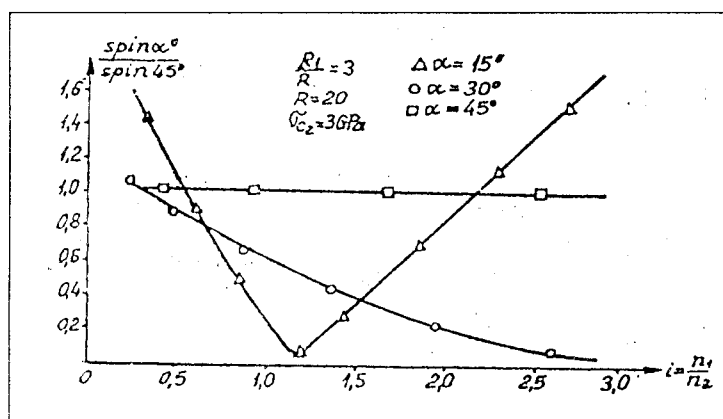
Figure 11. Spin relative variation; contact exit
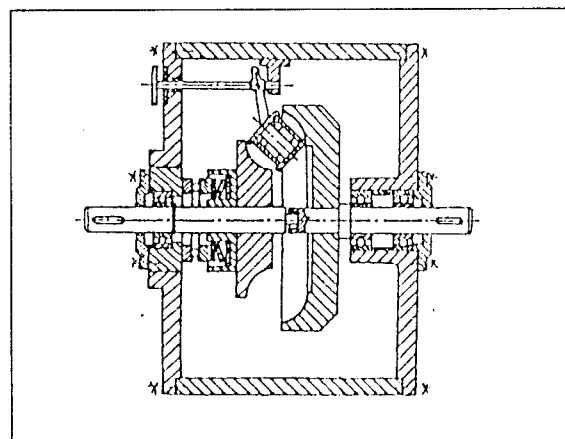
Figure 12. Improved Perbury traction drive

For $R_1/R = 0.5$, $\sigma_c = 2\,GPa$, taking for the entrance disc an angle $\alpha = 15°$, the spin is reduced for over 60 percent for a range of 5; as a mean value, the spin is diminished for over 40 precent for the whole range.

If the cones angle is 30°, only for a limited range the spin reduction is considerable, and yet, the spin is more diminished than in the intial variant, [1], [7].

In conclusion, the most favorable angle is $\alpha_{optim} = 30°$, not only by the above considerations, but also, by considering the fact that the use of this
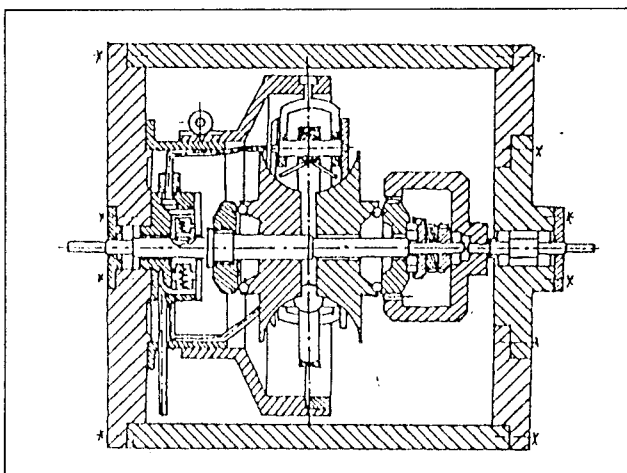
Figure 13. Traction drive with reduced spin

value does not complicate the ratio adjusting system. On the other hand, reducing the angle from $45°$ to $30°$ a decrease of the axial force value from the journal bearing occurs and therefore, a lessen of the losses too. The value $\varphi = 0.85$ for the conformity of the contact between the ball and the retain - lubricate ring, which ensures minimum rolling losses, is recommended, [1], [7].

5. VARIABLE RATIO, HIGH PERFORMANCE TRACTION DRIVES

As stated above, the reduction of active contacts is a very efficient solution to decrease the power losses in a traction drive. This idea led to two new designs of traction drives, namely an improved Perbury drive, shown in figure 12, and a reduced spin torical drive, illustrated in figure 13, [1]. These use double rollers that lead to a
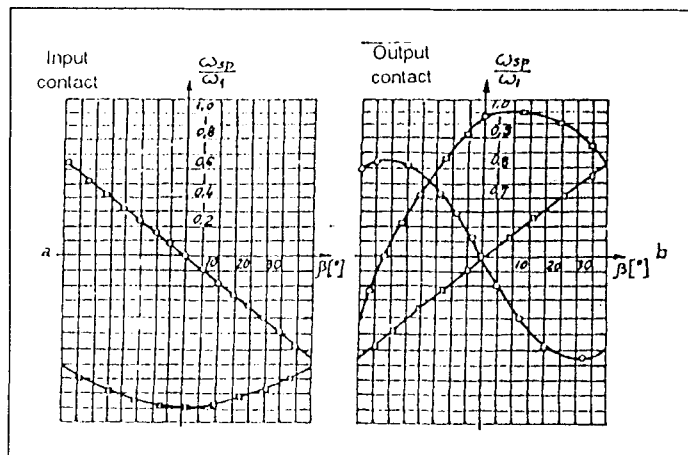

Figure 14. Spin - roll ratio in Perbury traction drives
□ classical version; ○ improved Perbury drive;
△ reduced spin drive

Figure 16. Performances of ball on disc traction drive with unloaded rolling bearings

decreased spin-roll ratio, a higher contact fatigue life and improved conditions of lubrication of both contacts. The corresponding analytical relationships are given in [7] and shown in figure 14.

Another efficient solution consists in an internal design of the drive based on unloaded main rolling bearing and on an incorporated oil pump for lubrication, [12]. Such a traction drive is shown in figure 15, [11]. As indicated in figure 16, the performances of the ball on disc traction drive are high. A different version of this design is shown in figure 17.
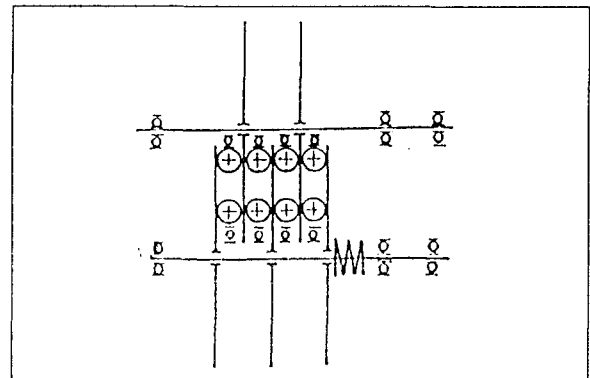
Figure 15. Ball on disc traction drive with unloaded rolling bearings

5. CONCLUSIONS

The following conclusions can be drawn as a result of the analysis performed above:

► improved performances of EHD traction drives require reduction of functional longitudinal sliding by use of special lubricants, of adequate cooling of the drive and a low treshold rolling speed just able to form a fluid form;

► higher performances of EHD traction drives are obtained if the spin - roll ratio in the active contacts of the drive is reduced by an adequate geometrical design of these components;

► a high precision machining and mounting is necessary to produce a high performace traction drive;

► when multiple parallel intermediate elements are used, these must be synchronised by carefully conceived mechanisms;

► normal contact load must be applied directly to the active elements in such a way that the main rolling remain unloaded;

► an internal oil pump to assure a correct lubricant flow through the contacts is essential for a high efcienty transmission;

► examples of improved versions of traction drives which incorporate these principles can be seen in this paper.

Figure 17. High efficiency ball on disc traction drive

REFERENCES

[1.] *I. M. Ciornei*, **Ph. D. Thesis**, Polytechnic Institute of Bucharest (1986) (in Romanian).

[2.] *D. R. Adam and W. Mirst*, **Frictional Traction in EHD Lubrication**, Proc. Roy. Soc. Lond. (1973), 332.

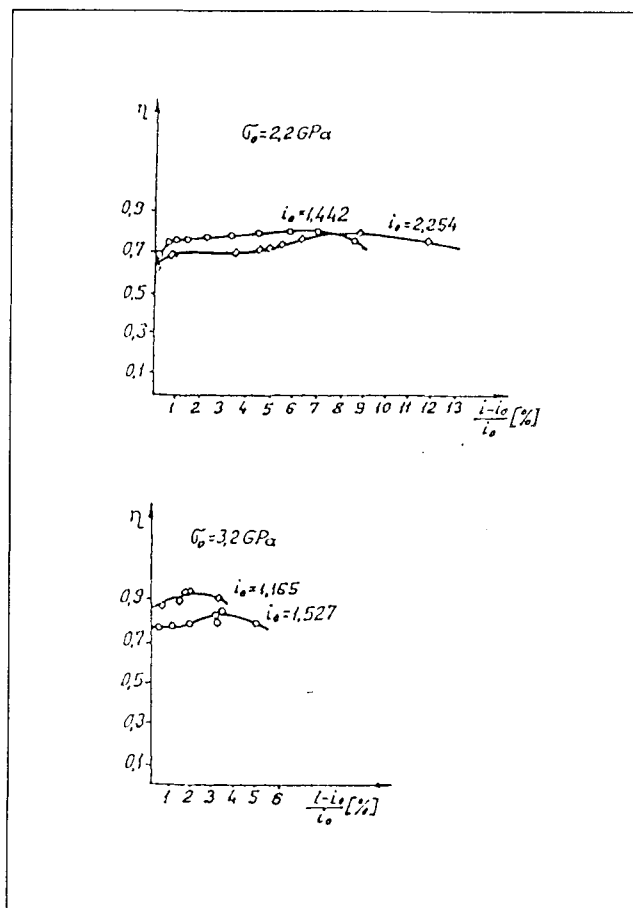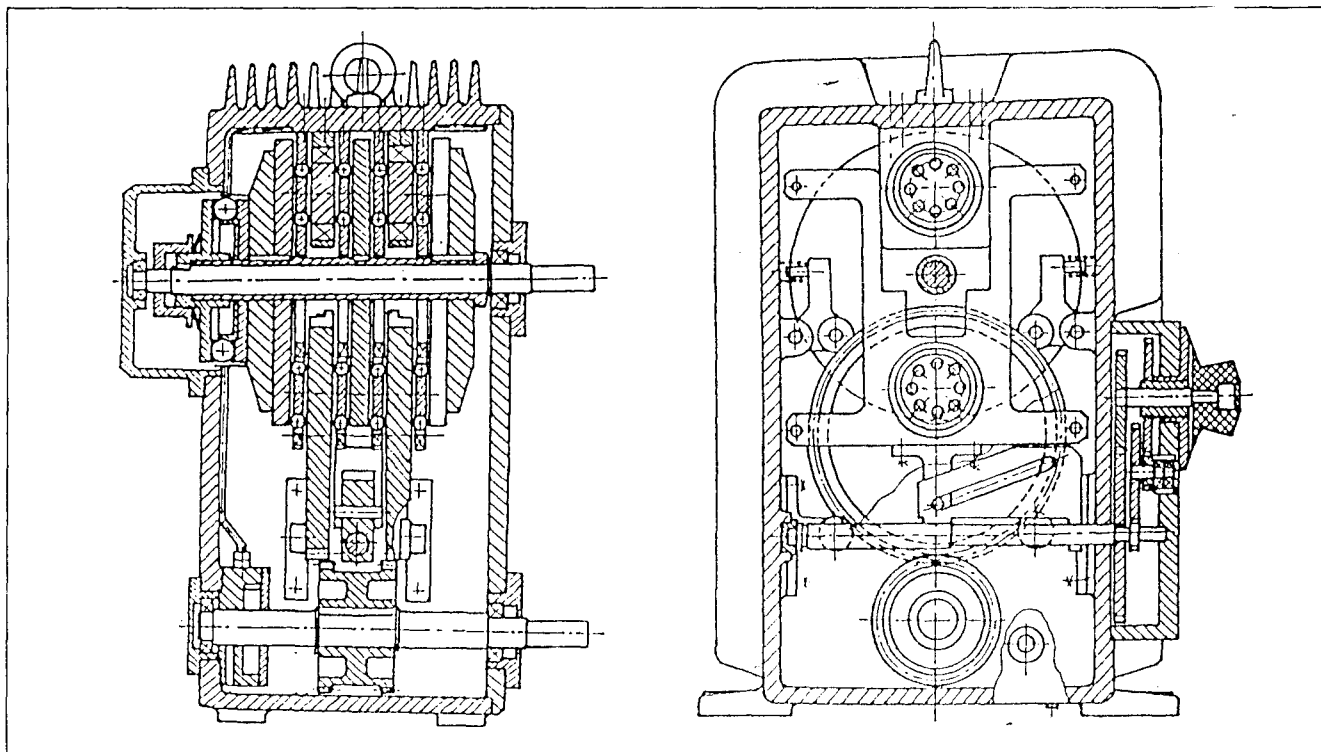[3.] *B. I. Klemz, R. Gohar and A. Cameron*, **Photoelastic Studies of Lubrication Line Contact**, Proc. Inst. Mech. Engs. (1971).

[4.] *O. S. Cretu*, **Ph. D. Thesis**, Polytechnic Institute of Iassy (1981) (in Romanian).

[5.] *E. N. Diaconescu*, **Ph. D. Thesis**, University of London (1985).

[6.] *R. C. Dutovski*, **Energy Bases of Balls Rolling an Ploters**, ASME, Series D, Journal of Basic Engineering, 81, (1959).

[7.] *I. M. Ciornei*, **The Optimisation of Perbury Traction Drive by Spin Reduction**, Proc. of The 5 - th European Trib. Congress, Eurotrib'89, vol. 5, p.100 -105, (1989).

[8.] *A. V. Sprisevschi*, **Rolling Bearings**, Masinostroenia, Moskva, (1969), (in Russian).

[9.] *W. Wenitz*, **Friction at Hertzian Contact with Combined Roll and Twist**.

[10.] *V. N. Constantinescu and I. M. Ciornei*, **On the Evaluation of Traction in Concentrated Contacts**, Acta Tribologyca, vol.I,1, (1992), p. 21-31

[11.] *E. N. Diaconescu , O. S. Cretu and I. M. Ciornei*, **Traction Drives**, **Proc. of the Seminar on Present and Future Trends in Research of Rolling Contact**, Suceava, (1985), p. 42-70, (in Romanian).

[12.] *E. N. Diaconescu and A. G. Crraur*, **Effect of Bath Oil Level Upon Performances of an EHD Traction Drive**, VAREHD 2, Suceava, (1982), p. 249-257, (in Romanian).

[13.] *I. L. Tevaarwerk*, **A Simple Thermal Correction for Large Spin Traction Curves**, ASME, vol.102, (1989), p. 440-446.

[14.] *I. L. Tevaarwerk and K. L. Johnson*, **The Influence of Fluid Rheology on the Performance of Traction Drive**, ASME, Jour. of Lubrification Tech., vol.101, (1979), p. 266-274.

[15.] *I. M. Ciornei*, **The Implication of Spin of EHD Traction Drives**, International Scientific Conference in Traction, Wear and Lubricants, Taskent, URSS, (1985), p. 22-28.

[16.] *E. N. Diaconescu and I. M. Ciornei*, **Traction EHD**, TCMM1, Editura Tehnica Bucharest, (1987), p.158-165, (in Romanian).

[17.] *K. Okamura*, **Mechanism and Performance of Traction Drives**, Japanese Journal of Tribology, vol. 35, no. 1, (1990), p. 23-33.

[18.] *I. Koizmui and O. Kuroda*, **Analysis of Damped Vibration of a System with Rolling Friction**, Japanese Journal of Tribology, vol. 35, no. 6, (1990), p. 733-739.

[19.] *M. Patterson*, **Traction Drive Contact Optimisation**, Proceedings of the 17-th Leeds, Lyon, Symposium in Tribology held at the Institute of Tribology, (1991), p. 295-300.

[20.] *A. Ishibashi, S. Hoyashita and H. Takedomi*, **Evolution of Efficiencies and Spead Ratios of CVT's with Planetary Cones**, Proceedings of the 17-th Leeds, Lyon, Symposium on Tribology held at the Institute of Tribology, (1991), p. 277 - 294.
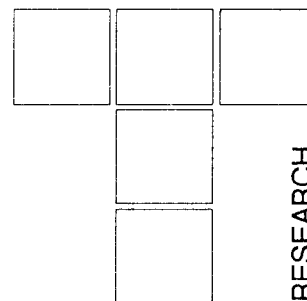
M. MILINOVIĆ, D. ŽIVANIĆ, P. AŠKOVIĆ

Friction Forces Influences In Multitube Rocket Launchers For Different Projectile Types

This paper considers theoretical and experimental aspect of unguided rocket projectile motion through the launcher of tube type. Major performances that influence shoot precision are initial rocket velocity and initial rotation (rpm) of projectile at launching tube muzzle. Both parameters are achieved by rocket engine forced motion.

Initial muzzle velocity is realized by total impulse of reactive thrust force, diminished by friction forces in launching tube. Initial rotation at tube muzzle could be realized by forced rocket motion through the screw gutter formed in the launching tube (one or more) or by space inclined nozzles driven by axial rocket thrust force.

Paper considers theoretical and stochastic experimental research of friction forces in static conditions. Boundary parameters that have influence on friction forces are determined. Average value and distribution of friction force is experimentally determined. Total influence of mentioned parameters is evaluated on the basis of experimental results.

Keywords: tribology, friction forces, launcher, unguided rockets, initial velocities.

1. INTRODUCTION

One of the most important parameters to obtain needed weapon performances, in the case of unguided rocket projectiles, is initial velocity (muzzle velocity), and also initial r.p.m at the lip of the launching tube. In fact, the most of modern artillery weapon systems have the tube type launchers as the best solution for unguided rockets. Multitube launcher is a weapon that has lower precision than classic guns and howitzers, but strong ripple fire, and speed of fire gives them important advantages. Above mentioned parameters have strong influence on precision and so, friction and friction forces become important factor during launching.

Achievement of rocket muzzle velocity and initial r.p.m. is realized by active motion through the launching tube using rocket engine thrust. This thrust is diminished by parasite drag that could be of impulse or continual type. Typical impulse parasite drag is rocket lock force in a launcher. Typical continuozes force, is a friction force, generated by all types of motion through the launching tube.

Two principal types to achieve r.p.m. of rocket, at the lip of the launching tube, are:

- the first type, by space inclined nozzles, that gives lateral component of thrust force. Distribution of few

Dr Momčilo Milinović, dipl. ing.,
Mr Dragoslav Živanić, dipl. ing.,
Predrag Ašković, dipl. ing,
Mechanical Engineering Faculty, Belgrade

nozzles around aft end of the rocket, gives rotational momentum generated by lateral forces of each of nozzles mounted on the aft end radii.

- the second type is the forced motion of the rocket caliber wedge through screw gutter. Active force moves rocket axial through launching tube, but rocket wedge that moves through screw gutter along the tube, gives additional rotation and at the aft end of the tube initial r.p.m. of rocket.

It is possible to realize two or more gutters along launching tube but it depends on design and type of rockets.

Friction forces in both cases are parasite drag that influence on initial muzzle velocity and r.p.m. losses, at the same time. Paper considers only the second type of initial rocket r.p.m. achievement.

There are two basic aims in this paper:

- the first is to evaluate appropriate mathematical model that gives relation between axial velocity and r.p.m. and friction forces joint with other forces.

- the second, to evaluate mathematical law and distribution law of stochastic nature of friction forces in real designed launchers.

The first aim always gives adequate evaluation of rocket initial velocity losses that is important factor for exterior ballistics and precision analyses evaluation. Also variation of friction forces gives possibility to realize calculation of maximum friction that represents threshold influence on needed performances, and to propose regulations for production control.

The second aim gives mathematical distribution and expected values, and, of course, statistical parameters necessary to evaluate qualities and properties of all tubes mounted on the rocket weapon. This is system integration and necessary data analyze about system behavior. This paper considers only screw gutter type of launching device, and it's theoretical and experimental model.

2. PHYSICAL MODEL

The most important initial parameters that gives initial stability of the rocket motion at the first active phase of trajectory, are initial muzzle velocity and initial r.p.m.

Major drag in launching tube is generated by friction forces. Lock force is a step form function and it is possible to take it in calculation before rocket motion. In spite of that, friction forces have stochastic character and also, sometimes, they are function of velocity of rocket.

Physical model of rocket with space inclined nozzles that provide initial rotation is shown in fig. 1. This physical and accompanying mathematical model could be explained with next few assumptions:

1. Active moment produced by rocket engine space inclined nozzles initiate rotating motion of projectile in launching tube. This active moment is produced by lateral component of thrust force that acts on projectile at the radius $d/2$ (fig. 1). Opposite to this active force acts tangential friction force $F_{\varphi tr}$ that acts uniform over the rocket perimeter of caliber $D/2$ (inside of the tube wall).

2. Axial motion is realized by axial component of thrust force (F_x) diminished by projectile weight $G \cdot sin\theta$ and friction force in launching tube F_{xtr} (axial friction force).
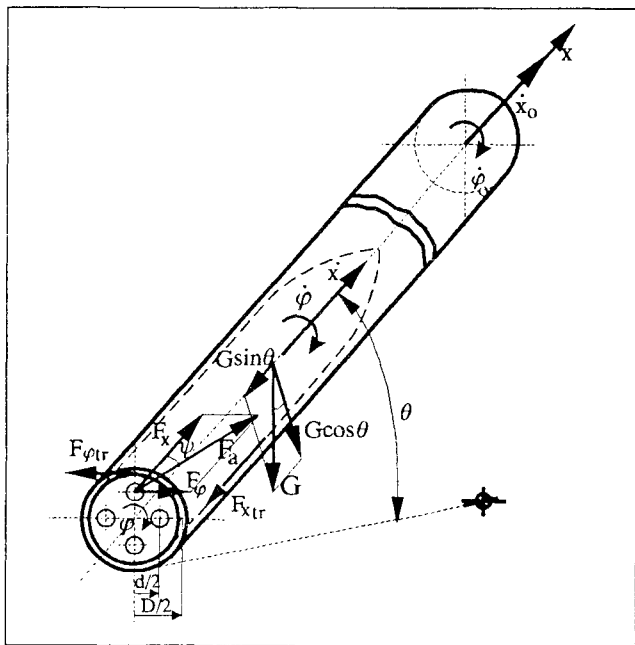

Figure 1.

3. Projectile motion is usually realized with constant thrust force F_a and nozzles are space inclined by constant angle ψ, relatively to the projectile axis. Launching tube is elevated for the fixed angle θ with respect to horizontal, so that projectile gradually changes potential energy during its motion toward the launching tube lip.

4. Projectile weight component $G \cdot cos\theta$ is normal force for both friction forces.

5. Friction coefficient is considered as independent of velocity in either axial or tangential direction for velocities up to $75\ m/s$. In velocities interval from 75 to $150\ m/s$ it is slightly dependent on velocity and this dependence has hyperbolic form.

Basic physical model, of screw gutter and caliber wedge system of launching, that provides r.p.m. of rocket rolling is shown on the fig. 2. This system is always used when higher caliber and higher ranges of unguided rockets are considered. Rockets of this type have booster engines or booster phase of sustainer engine, that realize (provide) impulse in a launching tube.

Principal feature of this system is to achieve r.p.m. by forcing wedge to move through screw tube gutter. Thus, physical model of resulting motion consists of axial rocket motion through the tube and rocket rolling along the tube axis.

Physical model of forces could be explained by next few states:

1) Axial thrust force generated by rocket engine is in the axis of rocket and launching tube. Opposite of rocket thrust acts $G \cdot sin\theta$ force, as a functional component of rocket weight G and active launcher elevation angle θ.

2) Three friction forces appear in a physical model. The first in contact of rocket with launching tube, rising up by normal component of rocket wedge, $G \cdot sin\theta$, and signed as F_{xTR} (fig.2).

   Second friction force appears as a component of total force in the screw gutter, generated by forced motion of wedge through gutter.

3) Perpendicularly on tube axis, but in the gutter, that means, tangentially on the tube diameter acts reaction of component of gutter perpendicular force. Gutter perpendicular force (fig.2), is equal to active force that initiates rolling of the rocket. This force arises due to rocket thrust force action and rocket wedge coupling with screw gutter, as a component of thrust force. This is composition of forces and its components in a screw gutter (angle of screw γ). Friction caused in a screw gutter is component force that acts on the active lateral side of gutter, during rocket wedge sliding.

4) Out of gutter, tangentially to the inside diameter of the tube, contact between rocket and inside tube surface generates new third friction force, caused by
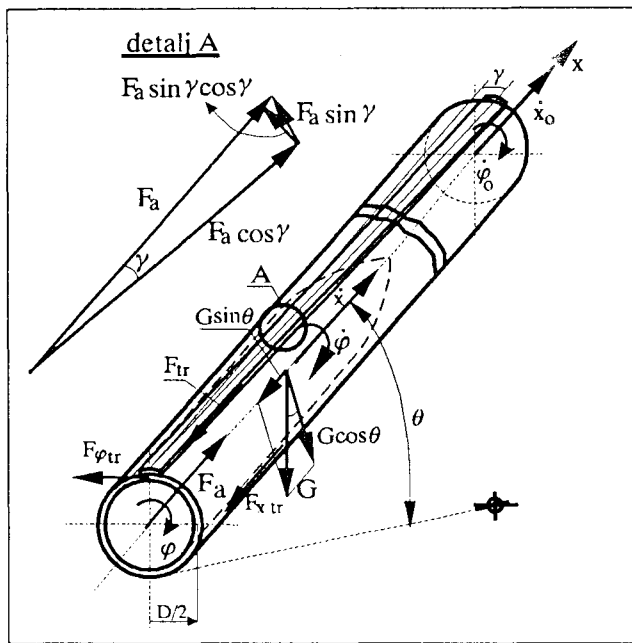
Figure 2.

rocket rolling. This is friction drag force due to rocket rotation $F_{\varphi tr}$).

5) Invariants of this physical model are next parameters:

▸ Thrust force generated by rocket engine (average value or unsteady state value, depending on adopted model).

▸ Weight G of rocket

▸ Elevation angle θ in vertical plane, of the tube with rocket,

▸ Angle of the screw symbol γ that directs gutter along the tube,

▸ Friction coefficient between rocket and launcher μ.

2.1 Friction Coefficient Analysis

At the very beginning of this research, friction coefficient was considered as a function of velocity in a simple form:

$$\mu = \frac{k}{V + \dfrac{k}{\mu_0}} \qquad (1)$$

In this equation coefficient k takes into account type of material and manufacturing quality of contact surfaces, eccentricity, etc. This type of equation gives general function form of relation between velocity and the friction force.

But, it is well known from previous research that in areas of lower speeds, friction coefficient is constant. Functional dependence expressed in form (1) is available only for areas of higher speeds between contact surfaces. That means that coefficient of friction keeps constant value in area less than threshold velocities that are about $75 \div 100$ m/s.

So, complete functional relation between velocity of surfaces in contact motion and friction coefficient, could be expressed in an approximate form as:

$$\mu = \begin{cases} \mu_0 & for\ V < V_{gr}\quad (75 \div 100\ ^m\!/sec) \\[2mm] \dfrac{k \cdot \mu_0}{k + \mu_0 \cdot (V - V_{gr})} & for\ V > V_{gr} \end{cases} \qquad (2)$$
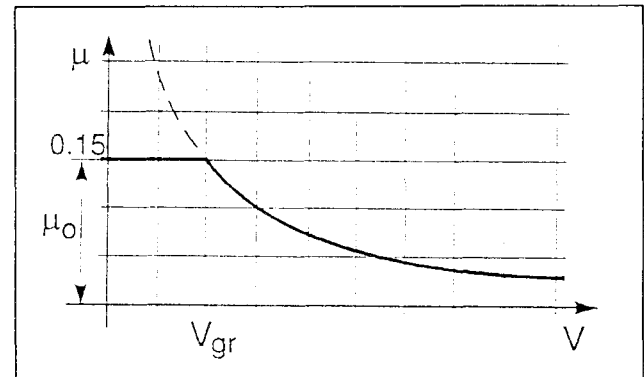
This form of equation is given on the fig. 3.

Figure 3.

But all that analysis gives poor (inadequate) results. Basic reason for that lies in fact that angle rolling for screw gutter type of rolling initiation is used always for r.p.m. numbers of about $600 \div 700$ r.p.m. Missile diameters (calibres), are usually less than 280 mm, so contact velocities values are about 10 m/s. Friction forces, generated by axial motion of rocket (along launching tube), take different velocity regimes. However, maximum velocities on the lip of the tube are about $80 \div 120$ m/s, so threshold velocities, in accordance with fig. 3 appear at the aft end of launchers. That reason is indicative enough to conclude that coefficient of friction in this launching system could be taken as approximate constant. That is reason why in above mentioned invariant parameters, friction coefficient also exists.

3. MATHEMATICAL ANALYSIS

Mathematical model is a solution of certain equations with next aim:

• To state relation between rotational and axial motion by velocity parameters.

• To form mathematical model where it is possible to take in consideration values of friction forces and distribution functions of forces, based on experimental research.

General purpose of mathematical modeling is to get dimensionless coefficients that have influence on initial r.p.m. and axial velocity of the rocket at the lip of the launching tube. General form of Lagrange's equations of II order that represents this type of problem is:

$$\frac{d}{dt}\left(\frac{\partial E_k}{\partial \dot{q}_i}\right) + \frac{\partial E_k}{\partial q_i} + \frac{\partial E_p}{\partial q_i} = Q_i \qquad (3)$$

where: $i=1, n$ (n - number of degrees of freedom).

For the first type of launching, shown in fig. 1, with space inclined nozzles, rotational motion is independent of axial. Lagranges equations of the second order, for generalized coordinates x and φ are

$$\frac{d}{dt}\left(\frac{\partial E_k}{\partial \dot{x}_i}\right) + \frac{\partial E_k}{\partial x_i} + \frac{\partial E_p}{\partial x_i} = Q_x \qquad (4)$$

$$\frac{d}{dt}\left(\frac{\partial E_k}{\partial \dot{\varphi}_i}\right) + \frac{\partial E_k}{\partial \varphi_i} + \frac{\partial E_p}{\partial \varphi_i} = Q_\varphi \qquad (5)$$

where equations for kinetic and potential energies are:

$$E_k = \frac{m \cdot \dot{x}^2}{2} + \frac{J_x \cdot \dot{\varphi}^2}{2},$$

$$E_p = m \cdot g \cdot x \cdot \sin\theta$$

and for generalized forces:

$$Q_x = \sum F_x = F_a \cdot \sin\psi - F_{xtr}$$

$$Q_\varphi = \sum M_\varphi = F_\varphi \cdot \frac{d}{2} - F_{\varphi tr} \cdot \frac{D}{2}.$$

Final equations of motion that result from this model could be considered in two ways, caused by different distribution of friction force in two segments of launching tube. These two segments conditionally could be named as low velocities segment, where friction force is independent of velocity, and high velocities segment, where dependence of friction coefficient on projectile velocity is given by equation 2.

Thus, for low velocities segment, final equations of projectile motion are

$$\ddot{x} = \frac{F_a \cdot \cos\psi}{m} - g \cdot (\sin\theta + \mu \cdot \cos\theta) = K_{Fx} \qquad (6)$$

$$\ddot{\varphi} = \frac{F_x \cdot \sin\psi}{2} \cdot \frac{d}{2} \cdot \frac{G}{J_x} \cdot \cos\theta \cdot \frac{D}{2} \cdot \mu = K_{M\varphi} \qquad (7)$$

For high velocities segment final equations of projectile motion are

$$\ddot{x} + \frac{C_1}{\dot{x} + C_2} + C_3 = 0 \qquad (8)$$

$$\ddot{\varphi} + \frac{S_1}{\dot{\varphi} + S_2} + S_3 = 0 \qquad (9)$$

where C_i and S_i are

$$C_1 = k \cdot g \cdot \cos\theta, \quad C_2 = \frac{k}{\mu_0}, \quad C_3 = g \cdot \sin\theta - \frac{F_a \cdot \cos\psi}{m}$$

$$S_1 = \frac{G}{J_x} \cdot \cos\theta \cdot k, \quad S_2 = \frac{2 \cdot k}{D \cdot \mu_0}, \quad S_3 = \frac{F_a \cdot \sin\psi}{J_x} \cdot \frac{d}{2}$$

Solution of final equations of projectile motion for the first segment gives velocity and angular velocity at the exit from the launching tube as:

$$\dot{x}_0 = \sqrt{K_{Fx}} \cdot \sqrt{2 \cdot l_0} \qquad (10)$$

$$\dot{\varphi}_0 = \frac{K_{M\varphi}}{\sqrt{K_{Fx}}} \cdot \sqrt{2 \cdot l_0} \qquad (11)$$

so that ratio of initial velocities of axial and rotational motion at the launching tube exit is constant and equal to the ratio of axial and angular acceleration,

$$\frac{\dot{x}_0}{\dot{\varphi}_0} = \frac{K_{Fx}}{K_{M\varphi}} = const = \frac{\ddot{x}}{\ddot{\varphi}} \qquad (12)$$

For the second segment solutions for $\dot{x}_0$ and $\dot{\varphi}_0$ are:

$$\dot{x}_0 = R_{1x} \pm \sqrt{R_{2x} - R_{3x} \cdot \tau} \qquad (13)$$

$$\dot{\varphi}_0 = R_{1\varphi} \pm \sqrt{R_{2\varphi} - R_{3\varphi} \cdot \tau} \qquad (14)$$

where: R_{1x}, R_{2x}, R_{3x}, $R_{1\varphi}$, $R_{2\varphi}$, $R_{3\varphi}$, are algebraic functions of constants C_1, C_3, C_3, S_1, S_2, and S_3 of differential equations obtained from (6) and (7).

For launching model shown in fig. 2, generalized coordinates q_i and generalized forces Q_i are expressed in a form, of moment acting on rocket:

$$Q_\varphi = \frac{D}{2} \cdot F_a \cdot (\sin\gamma \cdot \cos\gamma - \frac{\mu}{n} \cdot \cos\theta - \mu \cdot \sin^2\gamma) \qquad (15)$$

where $n = F_a/G$, is a relation between axial thrust and weight force.

Coordinates of axial motion x and rotational motion φ of rocket are not independent, so relation between axial velocity $\dot{x}$ and angular velocity $\dot{\varphi}$ is determined by screw gutter angle and diameter of gutter position on the tube. Then, well known relation of screw-narrow motion is expressed in a form

$$\dot{x} = \frac{D}{2} \cdot \tan\gamma \cdot \dot{\varphi} \qquad (16)$$

So it is possible to get kinetic energy equation only as a function of one generalized coordinate φ in a form

$$E_k = \dot{\varphi} \cdot \left[\frac{m}{2} \cdot \frac{D^2}{4} \cdot \tan^2\gamma + \frac{J_x}{2}\right] \qquad (17)$$

If we take time of launching (τ) as a known parameter, and if we suppose that acceleration in a launching tube has a constant value $\ddot{x}$, then initial angle velocity at the lip of tube becomes

$$\dot{\varphi}_0 = K_{M\varphi} \cdot \tau = K_{M\varphi} \cdot \sqrt{\frac{2 \cdot l_0}{\ddot{x}}} \qquad (18)$$

Final form of coefficient $K_{M\varphi}$ is a ratio between generalized force Q_φ and double coefficient of the derivative of kinetic energy in Lagrange's equation,

$$K_{M\varphi} = \frac{Q_\varphi}{2 \cdot C} \qquad (19)$$

Coefficient C is,

$$C = \frac{m}{2} \cdot \frac{D^2 \cdot \tan^2 \gamma}{4} + \frac{J_x}{2} \qquad (20)$$

Using Lagrange's equation or using axial to rotational coordinate transformation, we get the second derivative of axial coordinate (linear acceleration) in a form:

$$\ddot{x} = \frac{K_{\Delta Fx}}{2 \cdot H} = \xi \qquad (21)$$

This equation shows that total differences of friction forces and active forces expressed in a form of coefficient $K_{\Delta Fx}$ give constant acceleration along the tube. This opinion is supported by form of term H analogous with coefficient C and expressed in a form

$$H = \frac{m}{2} + \frac{2 \cdot J_x}{D^2 \cdot \tan^2 \gamma} \cdot \qquad (22)$$

Both equations (21) and (22) indicate that acceleration depend only of active forces, because all other influence parameters are constant. Final solution of muzzle velocity $\dot{x}$ at the lip of the tube (length l_0) is

$$\dot{x} = \sqrt{\xi} \cdot \sqrt{2 \cdot l_0}. \qquad (23)$$

Ratio between initial (muzzle) axial velocity and initial r.p.m. has form

$$\frac{\dot{x}_0}{\varphi_0} = \frac{\xi}{K_{M\varphi}} \qquad (24)$$

Using equation (14) we obtain final form of invariant coefficients

$$\frac{K_{\Delta Fx}}{2 \cdot H} \cdot \frac{1}{K_{M\varphi}} = \frac{D}{2} \cdot \tan\gamma \qquad (25)$$

This equation gives relation between forces of translation and rotation expressed in a form of inertial coefficients.In this case of launching ratio between rotation velocity of projectile and axial velocity is independent of friction in a launching tube, and depends only on geometrical parameters of launcher and screw gutter.

4. EXAMPLE

In calculation example shown in fig. 4 and 5. there are curves of the initial axial and angular velocities (r.p.m.). This case considers ideal type of launcher without friction forces and real with determined value of length l_0.
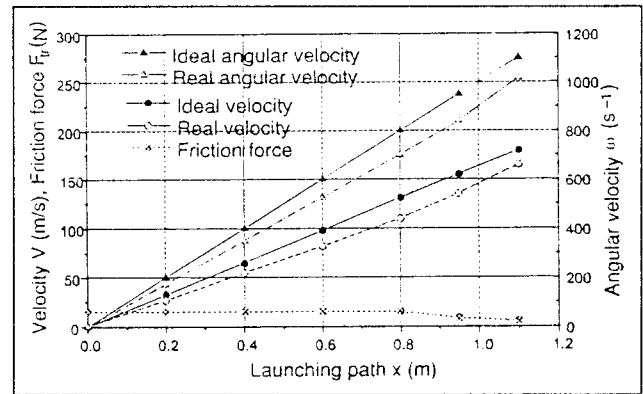
Figure 4. I case of launching

Distribution of axial and rotational velocity is given for real dynamic of launching.

It is important to notice that losses with respect to velocity and initial rotation, caused by friction forces for the first case of launching (in tube without screw gutter), have non-linear character only in the last segment of launching path. Diagram on the fig.4 shows constant value of friction force and non-linearity effect is neglected (disregarded). Active force in a launcher that generates acceleration of projectile is taken as a constant. So both curves, for real and ideal launching, have linear form (that means constant acceleration).
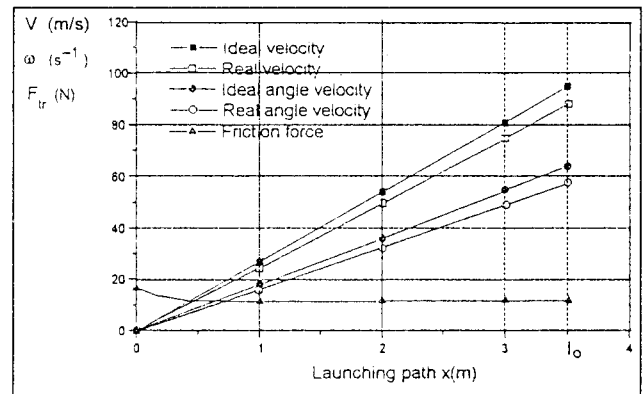

Figure 5. II case of launching

5. EXPERIMENTAL AND STATISTICAL RESULTS

During experimental research, force of friction has been measured by using real model of rocket. Model of rocket was towed through launching tube, and friction force was measured by extension dynamometer. This method gives friction force with the highest value of friction coefficient μ.

Experimental results have been reduced and shown in a table T1, with appropriate statistical values.

The diagram of normal law of distribution is shown in fig. 6.

It is visible (obvious) from diagram that number of experiments ($N=32$) is not enough to get good agreement with normal law of distribution. However, general form

of normal law of distribution is proved and experimental data for friction force distribution law is proved as a stochastic function.

Table T1

i number of points	value of friction force X_i [daN]	appearing number f_i (frequency)	average value $|X_i - X|$ difference [daN]	exponential parameter $t = |X_i - X|/\sigma$
1	16	1	5.1875	2.7600
2	17	0	-	-
3	18	3	3.1872	1.7019
4	19	1	2.1875	1.1674
5	20	6	1.1875	0.6337
6	21	5	0.1875	0.1000
7	22	9	0.8125	0.4300
8	23	5	1.8725	0.9600
9	24	0	-	-
10	25	1	3.1825	2.0346
11	26	1	4.8125	2.5600

Average value	$\bar{X} = \dfrac{\sum t_i \cdot X_i}{N} = 21.1875$
Standard deviation	$\sigma = \sqrt{\dfrac{\sum t_i \cdot (X_i - \bar{X})^2}{N}} = 1.8738$

But it is not possible to talk about friction force as random function, because calculation of dispersion shows other conclusions. In the table T2 are results of total percentages of friction forces in some dispersion tolerance fields.

Table T2

tolerance field	probability (or percent) of all appeared forces in a tolerance field	objection
± 2 daN	$P(X_1 < \bar{X} < X_2) = 0.71$ (71%) $x_1 = 19.18$ daN $x_2 = 23.18$ daN	given value of tolerance field
t = 1 that means ± 2σ	$P(\bar{X} - t\cdot\sigma < X < \bar{X} + t\cdot\sigma)$ $P = 0.9545$ (95.45%) $X_{min} = 17.44$ $X_{max} = 24.92$ $t\cdot\sigma = 2\cdot\sigma \approx 3.74\,daN$ $R = 2\cdot\sigma / X \approx 0.176$ (±17.6%)	given value of statistical dispersion

From table T2 it is possible to conclude, that in dispersion area (measured by force), of only ±17.6% of average force value, there are 95.45% of all measured values of forces. That shows excellent agreement with predicted theory that is possible to take into account all forces with error of about 15÷20%, by total effect.
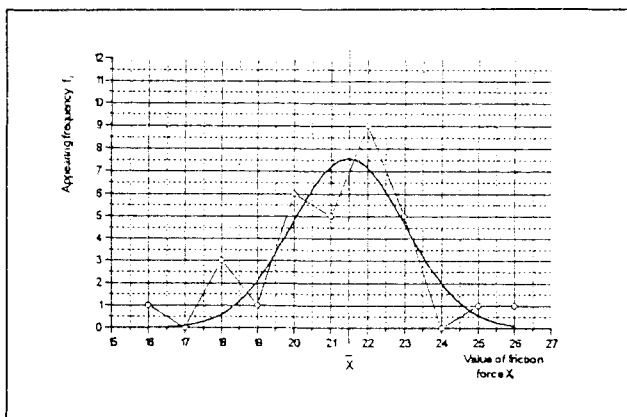

Figure 6

If consideration, that friction force is a small value compared to other forces, is taken into account, error of 20% (that is real), has not big influence on final results.

Experimental and statistical analyses proved that prediction.

6. CONCLUSIONS

Appropriate research was developed to describe physical, mathematical and experimental model of friction forces in a launching tube of multitube launcher.

Mathematical model shows relation between muzzle velocity and initial r.p.m., and also place and type of influence of friction forces in a tube, on these important rocket performances.

Experimental results, and statistical description of obtained data, shows normal law of distribution and possible tolerance field that contains 95.5 % of all friction forces that appeared during static test. That field is about ±18% up and down of average value of force measured in all tests. Error made in mathematical treatment is not of particular significance in that case.

Experimental results also gives data about necessary design parameters specially for tolerance field between dimensions of rocket to launcher integration. This tolerance field can be proved by measurement of friction forces tolerances (it's dispersion) and given as a regulations for final control.

LITERATURE:

[1] *Živanić, D.*, **Influence of self-propelled multitube rocket launcher oscillations on dispersion and cadence of launching**, master thesis, MF Belgrade, 1990

[2] *Milinović, M.*, **Principles of rocket and launcher design**, lectures, MF Belgrade, 1993

[3] *Slaymaker, R. R.*, **Calculation of slide bearings**, University of Belgrade, Scientific book, Belgrade, 1966

[4] *Vitas, D. J., Trbojević, M. D.*, **Machine elements**, Scientific book, Belgrade, 1981

LJ. TANOVIĆ

Processes Derived From The Diamond Grain Penetration Into Ceramics
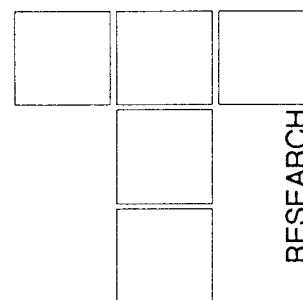
This paper is based on the number of hypotheses regarding stages of scrapings' formation during the ceramics' material processing, with special attention to the spotted processes. In order to make complex consideration of the occurred phenomena, there proceeded the process of micro-cutting using the separated diamond grain on samples of oxido-carbide (B3, BOK60) and nitrite (Silinit R) ceramics. The experiment was made with variable depth and penetration speed of the cone-shaped diamond grain of the tip angle $\beta = 120\text{-}160°$. The obtained results show that the mechanism of scrapings' formation is mostly influenced by lateral, radial and penetrating cracks. This paper also deals with possible equality between the processes of micro-cutting and hardness measuring at the grain pressing.

Keywords: ceramics, diamond, cracks

1. INTRODUCTION

The processing by grinding results as the summed effects of each abrasion particle, manifested through the deformation and destruction. However, in the processing area, micro-deformation and micro-destruction mechanisms differ, subject to processing parameters and non-uniform material to be processed (defects in the structure of material and defects occurring during processing). Still, there is no theory that would closely connect ceramic material micro-structure with the appropriate characteristics. Existing analyses regarding mutual connection always consider appropriate hypotheses. The occurrence of cracks may be spotted with two-phase ceramic materials with anisotropic heat expansion, or anisotropic elastic properties.

Papers by Takamia Y, Evans A.G., Heuer A.H., Cugo A., etc., deal with the study of ceramics' micro-structure. From their point of view, ceramics' defects are classified as: dislocations, deformations, pores, stages, grain sediments, segregation along the grain edge, and premises in form of hard solution.

At abrasion processing, the corresponding characteristics are submitted to significant changes due to the rate of the fastened abrasive hardness. Abrasive may be fastened hard of elastically, which changes the load distribution per grain, and therefore the penetration depth. Therefore, at the tools designing, we must consider permissible load per grain, as well as the fact that, in material, forces occurred at processing should form local stresses below the level of the destruction ones.

Doc. dr Ljubodrag Tanović
Mechanical Engineering Faculty, Beograd

2. HYPOTHESES REGARDING SCRAPINGS' FORMATION

Hypotheses regarding stages of scrapings' formation during the ceramics' processing are mutually different, even contradictory.

Nakajima, T., Uno, Y., Fujiwara, T., [4] have, at ceramics' samples Syalon and PSZ, during micro-cutting with variable depth, using the cone-shaped diamond grain, of the tip angle $\beta = 120°$ and $r = 5\text{-}30 \, \mu m$, spotted three depth zones: a) zone of elastic and plastic deformations, as well as the cutting zone; b) there is a critical depth and a normal force which corresponds to both plastic deformation beginning and cutting; and c) the diamond grain trace, formed as a result of plastic deformations and brittle erosion.

Salje, E., Mohlen, H. [6] suppose that, on the basis of type of the diamond grain chipping and connecting tissue, during the ceramics processing there occur "ripping" and "scraping" of the surface rather than ordinary scrapings chipping (figure 1). Such mechanism of the scrapings' formation is the result of the great material brittleness. According to their opinion, the diamond grain penetration is performed in three stages at metal processing. Contact stress between the grain and material is the most important for the scrapings formation. At grinding, the scrapings chipping may lead to slight connecting tissue erosion.

Inasaki, I. [1,2] has compared processing of brittle and resistant materials using the diamond grain and concluded that brittle material processing produces thin dispersion scrapings of different shapes. Such scrapings are result of cracks, at which the scrapings thickness may be bigger than the cutting depth (fig. 2).
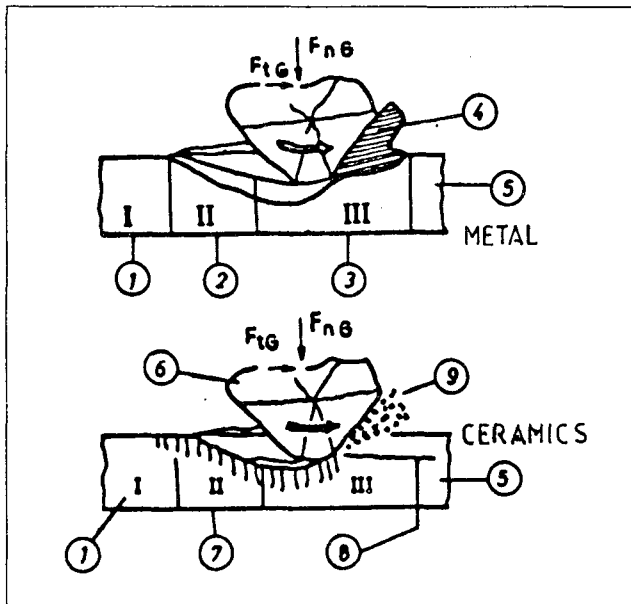
Fig. 1 Parallel presentation of the scrapings formation
at metal and ceramics processing
1 - elastic deformations; 2 - plastic deformations;
3 - scrapings chipping; 4 - scrapings; 5 - material
to be processed; 6 - diamond grain; 7 - forces
against softening; 8 - ripping; 9 - scrapings pieces

Hepworth, A.A., and Thompson, R., [5] suppose the similarity between the processing mechanism of ceramics and other materials, including titan and silicon alloys, hard to be processed.

Prins, J.F., thinks that during ceramics processing, there mostly appear both brittle material chipping and elastic deformations, grain chipping as well as the occurrence of micro-cracks.
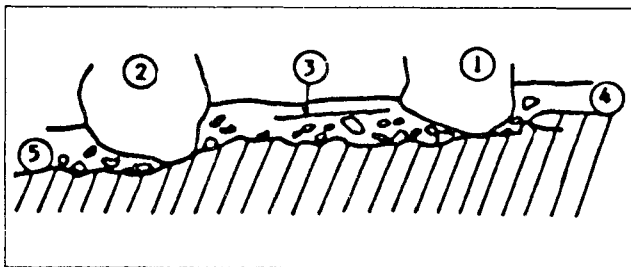

Fig. 2 Model of the scrapings' formation at
the ceramics grinding
1, 2 - abrasion grain; 3 - scrapings' pieces that passed
over the processed surface of the former grain;
4 - non-processed surface; 5 - processed surface

Thiel, N.W., stresses that, during the correctly conducted ceramics processing, there mostly appears ceramics grain chipping, which result is the occurrence of good surface topography.

Pluta, Z., starts from the fact that, at the coupling of two bodies, there appear stress and deformations which further cause cracks and chipping of full ceramics grains or its pieces. The result of the said is brittle cutting.

Lemener, A. [3] says that, due to the surface temperatures within the cutting zone, ceramics may become soft, and therefore, plastically deformed, and, as well as other materials, it is well processed with cutting.

Luroe, G.B. bases his theory on the scrapings' formation on the diamond grain penetration depth through the processed material. At small penetration depth, there exist elastic deformations as well as friction, while, at bigger one, there exist plastic deformations which, at certain moment, cause the occurrence of scrapings.

Imanaka, O., Fuyiuo, S., Mineta, S., have compared the scrapings' formation at brittle and resistant materials and concluded that, at brittle material processing, there appear thin - dispersion scrapings.

3. PROCESSES DERIVED FROM THE DIAMOND GRAIN PENETRATION

For the purpose of complex study of processes derived from the diamond grain - ceramics contact, researches are organized in two directions: 1) realization of the stand for micro-cutting process under regular grinding regime, and 2) identification of the grain pressing process at hardness measuring with the diamond grain work inside the whetstone.

Taniguta [1, 2] has, in his researches, pressed the grain with sharp and oval tip into brittle and resistant material, and analyzed occurrences derived in this way, figure 3. During the penetration of the oval tip grain through brittle material, there appear cone shaped cracks along the contact zone edges, expanding through the brittle material body. Regarding plastic material under the analogue conditions, there appears grain shaped crater with outlets along edges. During the penetration of the grain with small radius of the oval tip, and at slight forces, on both materials only plastic deformations may be spotted. At penetration of sharp grain into brittle material there appear cracks in direction of penetrating, as well as in other directions.

The occurrence of these cracks is explained with the presence of initial cracks in brittle material, i.e., cracks which are connected to the ceramics material structure. At penetration of such grain into plastic material, material behaves the same as in case of penetration using oval tip grain.

Such research is characterized by two phenomena: no methods, which would enable separation of the initial cracks from the ones occurred in the process, have existed so far; grain penetration considers no deformation rate effects.

For the purpose of reaching the highest level of inspection in the phenomena derived from the diamond grain-ceramics contact, the micro-cutting process is performed

Condition \ Material	Brittle	Plastic
Bigger Oval Radius		
Smaller Oval Radius — Smaller Load		
Smaller Oval Radius — Bigger Load		

1 - Elastic Deformations
2 - Plastic Deformations
3 - Cracks

Fig. 3 Deformation and erosion model at the grain penetration

with separated cone-shaped diamond grain ($\beta=120$-$140°$), at the penetration speed of 35 m/s. The said process was performed at samples of cutting ceramics of trade marks as follows: B3 ($\rho=4.50$ g/cm3, 92 HRA, $\alpha=6$-$6.1\cdot10^{-6} K$), BOK 60 ($\rho = 4.2$-4.3 g/cm^3, 92-94 HRA, $\alpha=6$-$6.2\cdot10^{-6}$ K), and SILINIT R ($\rho=3.8$-4 g/cm^3, 94-96 HRA, $\alpha=2.7$-$3.0\cdot10^{-6}$ K). The inclination of ceramics samples was 1:200, in relation to the grain motion, in order to enable the micro-cutting with variable penetration depth.

The analysis of traces derived from micro-cutting process using separated diamond grain enabled to put forward the hypothesis on stages of the scrapings' formation. At smaller grain penetration speed, there occur plastic deformations of the ceramics grain tips, because of the penetration depth which is above the value of the mean ceramics grain size. Thus, there exists the overcoming influence of normal cutting force component, which causes the pressure state. At the same time, the presence of the tangential force component leads to the plastic deformations of the grain tips, which take the shape of peelings arranged one above the other, and oriented in motion's direction. At greater penetration speed, normal and tangential resistance components grow, which may cause the ceramics grain destruction (crushing), and further, it may lead to the occurrence of the thin-dispersion scrapings (figure 4). The ceramics grains chipping is also spotted, as the consequence of a position in the structure, although - in case of grinding process - it may be explai-

Fig. 4 Stages in the ceramics grain chipping

ned by the irregular geometrical shape of the diamond grain and by possible process of "ripping", i.e. "scraping" of the coupled surfaces of ceramics-diamond grain. There also exists the phenomenon of total ceramics grains' withdrawal, yet in small extent.

As the consequence of great ceramics brittleness, plastic deformations are followed by lateral, radial and penetrating cracks. It should be stressed that the micro-cracks are spotted in case of multistage ceramics materials with anisotropic heat expansion or anisotropic elastic properties. The most outstanding is the occurrence of radial cracks (figure 5), which are, through penetrating speed and depth, getting bigger up to the critical level, at which they are gathered together (figure 6).

Then they cause the material withdrawal in form of blocks, unequal in shape and size. This way of the scrapings' formation is the most frequent, therefore these researches develop for the purpose to find the boundary penetration depth at the given speed, producing this
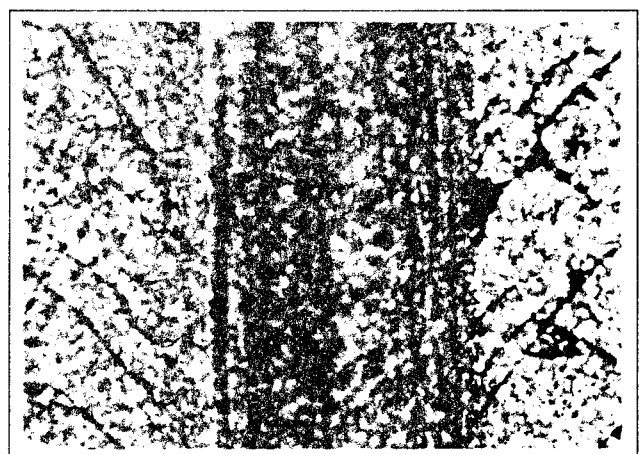

Fig. 5 Formation of radial cracks

*Fig. 6 The instant of cracks' gathering
(Silinit R, β = 140°C, Vs = 23 m/s)*

scrapings' formation mechanism. The results show that, at the ceramics micro-cutting, B3 boundary penetration depth varies within $7\text{-}9 \, \mu m$, BOK 60 $7\text{-}12 \, \mu m$, and Silinit R $4\text{-}12 \, \mu m$, regarding the penetration form and speed. There are few sources regarding limit forces at which cracks appear. Inasaki [1, 2] has, through experiments, come to the dependence:

$$F = \frac{\alpha \cdot K_{Ic}^4}{HV^3} \qquad (1)$$

Where: α - coefficient which includes shape of the grain with which the cutting process is performed;
K_{Ic} - resistance of materials against cracks.

Taniguta has come to theoretical and critical loads F_k and F_r at which square and radial cracks appear.

$$F_k = \frac{\alpha_k \cdot r \cdot K_{Ic}^2}{E} \; ; \qquad F_r = \frac{\alpha_r \cdot K_{Ic}^4}{HV} \qquad (2)$$

Where: α_k, α_r - non-dimensional constants
r - grain tip radius.

If we knew critical load of ceramics material, we would be able to perform grinding without new cracks.

4. CONCLUSION

On the basis of the obtained results it may be concluded as follows:

► Processes derived within the zone of ceramics cutting have not been cleared enough yet.

► Mechanism of the scrapings' formation includes processes of elastic and plastic deformations, scraping, chipping and withdrawing ceramics grains, as well as grains crushing which cause the occurrence of dispersion scrapings.

► There also exist lateral, radial and penetrating cracks, which are stretched out under the appropriate angles with respect to direction of the diamond grain penetration.

► There is also determined the diamond grain boundary penetration depth, at which the cracks are gathered, and therefore scrapings are formed on the samples of cutting ceramics B3, BOK60 and Silinit R.

REFERENCES

[1.] *Inasaki, I.*, **Grinding of Hard and Brittle Materials**, CIRP Ann., v. 36/2, 1987, 463-471

[2.] *Inasaki, I.*, **Spee-Stroke Grinding of Advanced Ceramics**, CIRP Ann., 1988, 29-302

[3.] *Lemener, A.*, **Oberflächentopographie und Festigkeit von Keramik nach der Schleifbearbeitung**, Industrie Diamanten Rundschau, 23, 1989, 2, 96-101

[4.] *Nakayima, T., Uno Y. i Fujivara, T.*, **Cutting Mechanism of fine Ceramics with a single Point Diamond**, Prec. Eng., 11, 1, 1989, 19-25

[5.] *Pluta, Z., Kacalak, W.*, **Mikroskopische Untersuchung von Diamantkörn-Spanspuren auf Aluminiumoxid-Keramik**, Industrie Diamanten Rundschau, N3, 1983, 124-130

[6.] *Salje, E. i Mohlen, H.*, **Prozessoptimierung beim schleifen keramischer werkstoffe**, Industrie Diamanten Rundschau, 1987, 243-247

[7.] *Tanovic, Lj.*, **Cutting Ceramics, Properties, Manufacturing and Processing by Grinding**, Faculty of Mechanical Engineering, Belgrade, 1992.

[8.] *Tanovich, Lj. i Ryzhov, E.*, **Studies of Microcutting Ceramic Materials**, Sverhtverdie materiali, Naukova Dumka, 1994, N1, 49-53
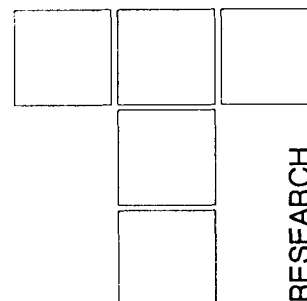
M. VELJIĆ, Đ. ERCEGOVIĆ, V. ĐORĐEVIĆ

Application of Protective Coating Against Wear of Soil Treating Agricultural Machinery Tools

RESEARCH

Specifics of soil tillage require solving of few questions related to realization of agrotechnical demands, decreasing of energy consumption and increasing of lasting period of usage. This paper gives the analysis of causes and wear intensity of soil treating agricultural machinery tools at different working conditions. Applying of carbon and alloy steels of different hardness was considered. Our experiments present the results related to application of metal coating on the surfaces of soil treating agricultural machinery tools. The experiments showed that hard metal coating on the cutting edge of tool significantly increase wear and changing of tool geometric form. It shows that applying of this procedure is justified.

Keywords: metal coating, wear, tools, steel, soil.

1. INTRODUCTION

The soil treatment is one of the most responsible operation of the agricultural producing process. Some rough estimations show that this part of the process takes about 40% of all input energy. More economical applications of the soil treatment machinery can be observed through development of all tools and working parts. They must provide high degree of all agricultural demands as well as the lowering of the pulling force, to provide long lasting period of usage and to enable lower exploitation and maintenance costs.

Characteristics of passive tools is a larger surface in contact with soil, because the soil tillage is being done by cutting and sliding of soil layer over the working surface. In active tools, particularly driven, cutting, crumbling and trowing soil away are done by knife or bolt. Common characteristics of all tools are wear, dulling of cutting edge (plowshare, knife, disc, tine) and wear of working surface (mouldboard, plough body, disc body).

Variety of shape, dimensions, way of soil treating, different working conditions (type and state of soil), shows a complexity of problem connected with designing and producing of tools for soil tillage. Wear causes change the tools constructive parameters, so the substitution of tools is often necessary after a short working period. Fast wear of components demands money spent for their

Prof. Milan Veljić, PhD,
Faculty of Mechanical Engineering, Belgrade
Prof. Đura Ercegović, PhD,
Agricultural Faculty, Belgrade
Prof. Vitomir Đordević, PhD,
Faculty of Mechanical Engineering, Belgrade

maintenance, producing of spare parts and effects jams, decreasing working effects, relatively using period of agricultural machines.

Coating with metal materials, with a low friction, resistant to wear, should enable tools production of cheaper low carbon percentage steels.

2. WEAR OF TOOLS

Wear of the working surfaces is the consequence of soil particles with sharpen edges sliding down the metal. Quartz particles have the highest hardness and they are a part of most sandy soils, clay soils have lower hardness and their wear has a lower intensity. During the sandy soil tillage, total wear of mouldboard occurs after 50-70 ha and of the plowshare after 10-15 ha, during the loam tillage wear of mouldboard occurs after 200-500 ha and wear of the plowshare is very low and change is rarely needed.

The wear intensity of the surfaces of soil treating agricultural machinery tools, besides numerous influencing factors, depends a lot on soil humidity. Figure 1. shows dependence of wear intensity and humidity for different soil types: 1 - sandy soil; 2 - sandy loam; 3 - light loam; 4 - clay soil. With humidity increasing in determined interval (curve 1 and 2), soil particles adhesion increases, that causes relative sliding and wear increasing. Further humidity increase reduces adhesion force of soil due to surface stress decreasing, and causes wear reduction.

Also velocity of soil particles moving over a working surface has an influence on wear of plough body working surface. For better interpretation of influence that the
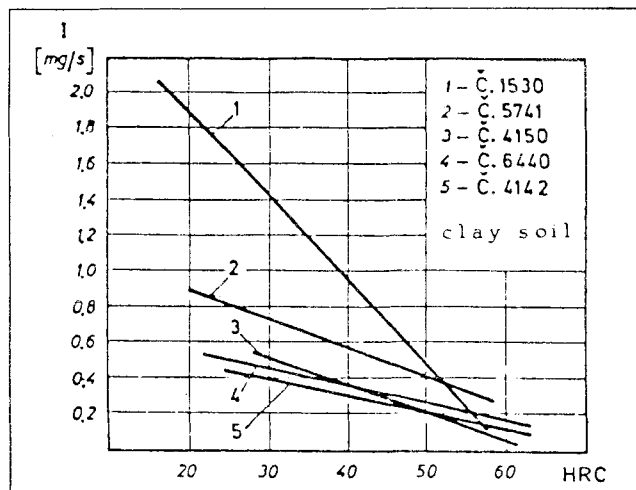
Figure 1. Relation between wear and humidity

working velocity of plough has on wear, the average values of plowshare wear in particular points were measured, figure 2., after the tillage of 4 ha sandy soil with humidity 6.65-8.5 %. Changing of wear in dependence of velocity for few chosen points is given on Figure 3. Increasing of motion speed from 1.25-3.33 m/s causes fast increasing of wear in the points nearer to cutting edge, and increasing of distance to the plowshare peak causes gradually decreasing of wear. By the magnitude of wear increasing, plowshare could be divided into three zones: I - the front side, II - cutting edge, III - the back side.

With the change of plough motion velocity, mouldboard wear per thickness changes in different points, figure 4. The investigations showed that, in sandy soil tillage,
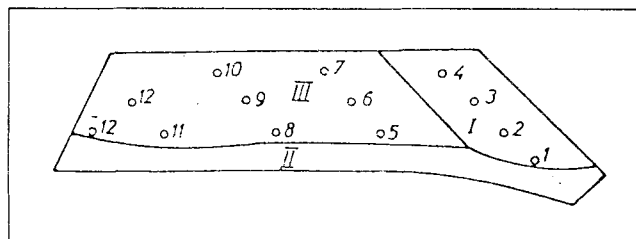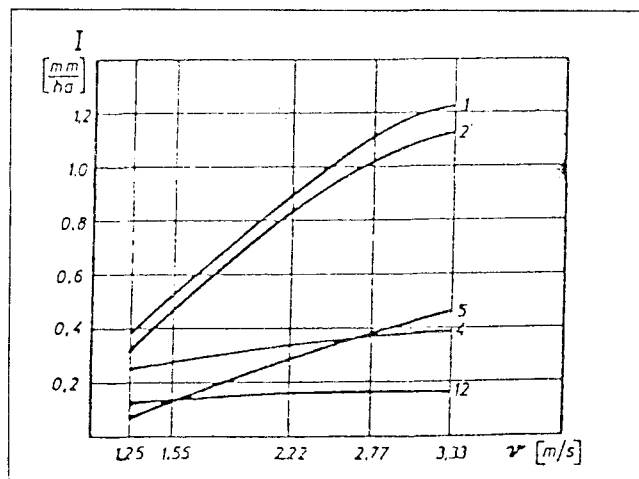

Figure 2. Zones and measuring points on the plowshare

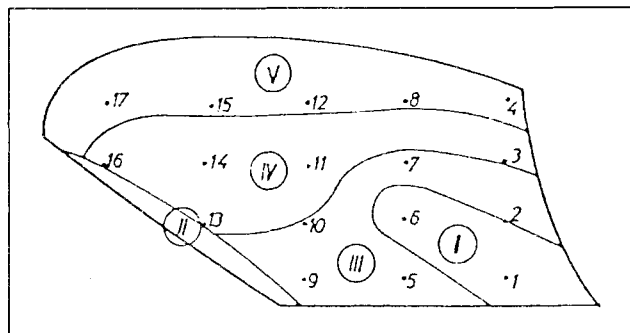Figure 3. Relation between wear and motion speed

Figure 4. Zones of wear and measuring points on the moul-

mouldboard has a large wear on the front part in the zones I and III, while the wear is insignificant in zone V.

Nonuniform wear of working surfaces is caused by various specific pressures on working surface, relatively to various strains and ways of particle removing. It could be concluded that where the pressures are the highest the wear is the biggest, but it's necessary to take into consideration an influence of particle slide velocity. Figure 5. shows the distribution of specific pressure per vertical contour lines of plough body working surface, during the work on clay soil, humidity 12 - 16 %, compression - penetration resistance 14-16 bar. It is established that the biggest pressure has the plowshare peak, while on the last side pressure is lower for 40-50 %.
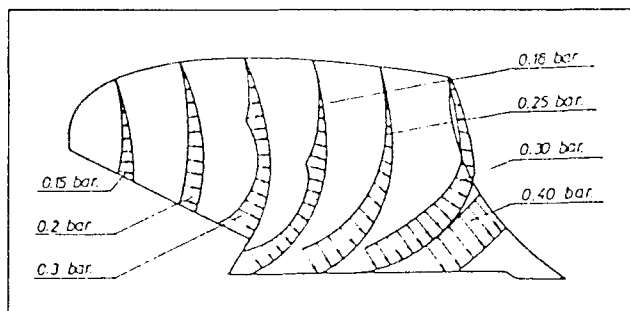
Figure 5. Distribution of specific pressure per vertical contour lines

As a result of soil abrasive action on agricultural machinery tools, wear of their cutting edges appears and causes dulling. It increases pulling force, spoils motion stability of machine, deteriorates weed curtailing. This causes deterioration of tillage quality and bigger energy consumption.

3. MATERIALS USED FOR SOIL TREATING TOOLS

Materials that are used for soil treating tools are mostly carbon steels with 0.45-0.65 % C, alloy steels with necessary heat treatment or three-layered materials. Contemporary heat treatment technology, so-called "isothermal quenching" and its different variants, are used for heat treatment of agricultural machinery tools.

Figure 6. shows the dependence between wear of the alloyed steels of various structures and hardness, compared to the carbon constructive steel Č.1530, which the agricultural machinery tools are often made of, during the tillage of clay soil with humidity 5-7.3 %. It can be concluded that with the hardness increasing of heat treated steels wear decreases. Č.1530 steel lowers its wear 5 times when its hardness is increased from 40 to 55 HRC while alloyed steels lower their wear 2 times, that means wear is lower for the lower hardness. The investigations showed that arrangement of wear for different soils is not same, what shows that hardness is not the only indicator of wear. Improved resistance to wear of alloyed steels is caused by the presence of alloying elements: manganese, nickel, chromium, molybdenum, tungsten and titanium. Alloying elements influence the steel structure making ferrite; manganese and silicon are dissolved in feritte and in that way improve hardness and strength; nickel increases hardness but doesn't provide lower friction; chromium used in steel in less quantity makes hard carbides which improve hardness and wear resistance; tungsten and molybdenum don't have a big influence on hardness improvement but provide a lower friction.
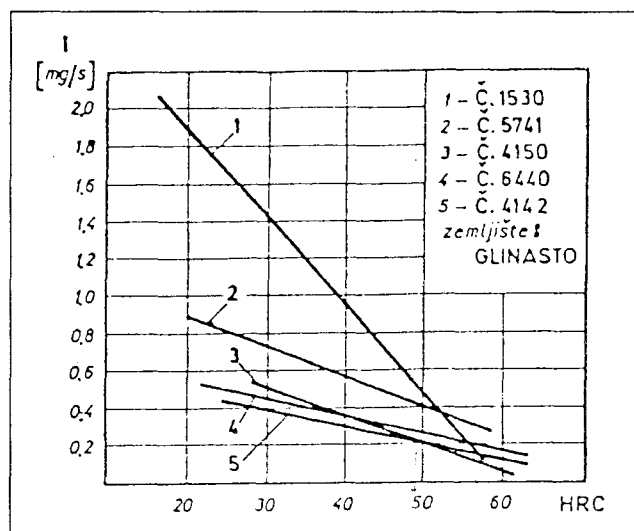

Figure 6. Relation between wear and hardness

For one-layered mouldboard, steels with 0.47-0.53 % C; 1.2-1.4 % Si and 0.7-0.9 % Mn are used. The mouldboard of three-layered steel, where the medium layer is made of mild carbon steel with thickness of 2.3 mm and the exterior - hard layers with a thickness of 1.8 and 3.5 mm, are mostly made of alloyed steel with hardness of 46-50 HRc.

4. POSSIBILITY OF FRICTION AND TOOL WEAR REDUCTION

In order to decrease friction and wear, the investigations of applying new constructing solutions and new materials were done. At the construction and production of tools, often are used solutions with many easy changeable com-ponents adapted to the zones of increasing wear. Due to avoiding fast wear that occured only in limited zones of mouldboard working surface and need for changing after a short period of exploitation, mouldboard is made of two or more parts, applying more qualitative and more expensive materials resistant to wear for more loaded parts (front part of mouldboard). Besides, the plowshare as well the landside and slade are often made of two easy changeable parts with different characteristics of material.

Vibrated plowbodies showed decreasing of needed pulling force during the lower speeds, due to free part of water enable easier sliding but also a structure damage and compression of the layer in contact with surface of plowshare and mouldboard at wet soil tillage.

At the latticed plowbodies, decreasing of mouldboard working surface up to one-third of whole surface is released. Back side of plough body is made of stripes, the decreasing of pulling force is released by, and made it easier and more economical to maintain due to possibility of only particular stripes changing. Parallel measuring of pulling forces for normal and latticed mouldboard, without a complex analysis, showed that resistance of pulling on the depth of 26 cm is lower for 8 % and on the depth bigger than 35 cm is lower for 15 % at the latticed mouldboard in the investigations on the sward, with soil humidity of 18.2-19.8 %.

5. APPLICATION OF COATS AND THE RESULTS OF INVESTIGATIONS

Technologies of coating are begun and developed in last 30 years in different industries, such as: decorative coatings, microelectronics and metallurgic coatings. All of them use similar technics which, by the time, although with different approaches to the problems, release common solutions.

In application of coatings resistant to wear, usually material in the shape of wire or silt, that is coated in the dissolved station, is used. Between the mostly used procedures, it is needed to mention the following:

• procedure of thermal spraying coating

• procedure of electric arc coating

• procedure of plasma arc coating.

The investigations had a purpose to choose metal coatings most suitable for application at agricultural machinery tools, particularly for the zones of high wear. There were used 6 different coatings and their data about chemical structure and hardness is given in the table 1.

Coat	C	Si	Fe	Cr	Ni	B	W₂C	Hard ness
	%	%	%	%	%	%	%	HRc
Nº 1	0.03	2.30	0.40	-	Rest	1.30	-	18
Nº 2	0.35	3.70	1.70	8.50	Rest	1.80	-	45
Nº 3	0.75	4.30	3.50	15.00	Rest	3.10	-	62
Nº 4*	0.38	2.15	1.75	7.50	36.67	1.55	50%	65
Nº 5	0.38	2.15	1.75	7.50	36.67	1.55	50%	65
Nº 6	0.15	2.50	2.50	10.00	Rest	2.50	-	35

*extra hard

The establishment of wear of soil treating agricultural machinery tools included cultivator tools - tines. The operating of tines made of steel Č.1741 (8 pieces) and those ones where on the cutting edges are used the coatings of various characteristics were examed in working conditions. Additionally, fusion of coated layers was done. All tines are alternatively put on the cultivator. The cultivator worked on different types of soil. Layer thick 0.1 - 0.2 mm is coated on the cutting edges of tines in the stripes wide 15-20 mm, what is shown on figure 7.
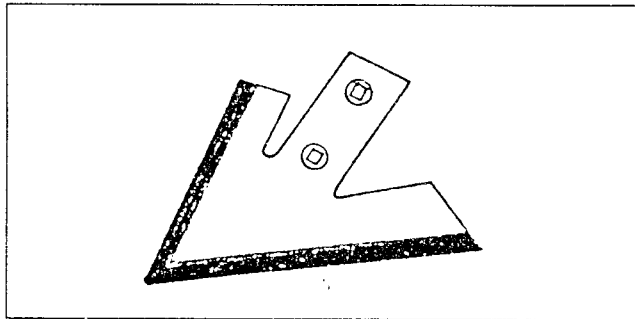

Figure 7. Tine with coated edges

By measuring of wear (mass loss) at the tines made of steel, it is established that wear was 173-277 mg and the average wear was 224.25 mg per tine, table 2. It is also established that all tines made of steel have the significant wear on the tines cutting edges and outstanding roundness of tine peak has occurred. This roundness of tines has a negative influence on the applying quality of agrotechnical demands and causes fast increasing of pulling force. The tines that have cutting edges with protective coating No 1 of hardness 18 HRc, have the same wear noticed as those made of steel Č.1741 without protective coating. When hardness of applied coating is increased, wear rapidly decreases and on the coating Nº 3 wear is almost 10 times lower than on those made of steel and this relation is much bigger if the coating Nº 4 is applied. Low wear of the coating Nº 6, although having the low hardness, could be explained by some lower friction and consequently by wear decrease.

Tine	Steel and coats [marc]	Hard ness	Tine mass		Mass loss
			before the testing	after the testing	
-	-	HRc	kg	kg	mg
1-8*	Č.1741	40	1.2004875*	1.1780625*	224.25*
9	1	18	1.2078	1.1860	218
10	2	45	1.1640	1.1528	112
11	3	62	1.2041	1.2108	23
12	4(1)	65(18)	1.2105	1.2069	36
13	4	65	1.2000	1.1988	12
14	4	65	1.2061	1.2046	15
15	5	65	1.2050	1.2013	37
16	6	35	1.1966	1.1956	10

*average values

Good results are reached when wolfram-carbid coatings are used on the cutting edges of the plowshare and mouldboard. These layers have the resistance to shock loading and after the coating they prolong the period of usage 3-5 times. However, analysis of this coating shows that when the humidity is low it has the same friction as those made of steel Č.4320, but when the humidity is higher, its friction increases related to steel Č.4320. This is the reason why the protective layer of Cr-Ni coating, thick about 250 μm is applied over this coating. Figure 8. shows the coating of the plough body working surface. Coated surface, stripe width is 25 mm, is previously shot blasted and afterwards part of surface, which borders on the coated stripe, is covered.

Spherical discs have the highest wear in the zones where the pressure and sliding speed are the highest, so the coating should be placed on the rim of the disc in the stripe width 25-30 mm, figure 9.

When the Cr-Ni coating is applied on the cutting edge of the tine, width 25 mm, it is desirable to apply the heat treatment of the tine peak.
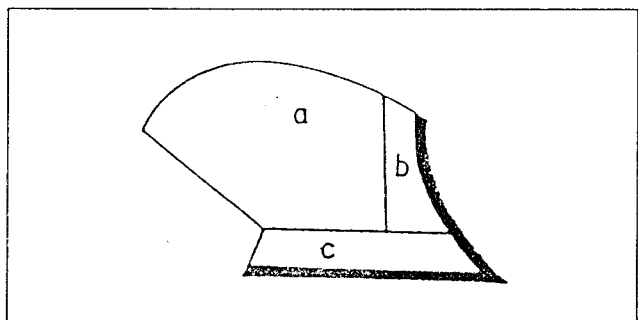

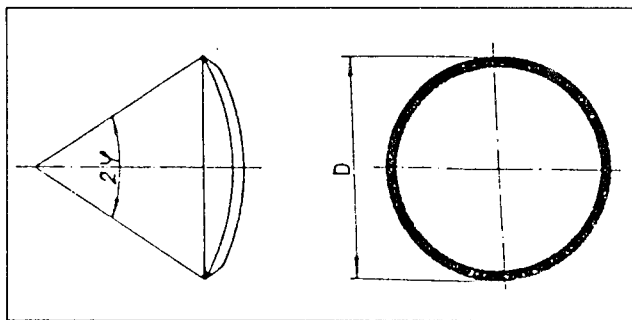*Figure 8. Coating of the plough body working surface*

Figure 9. Coating of the spherical disc surface

Results of investigations show that coated tines with heat treatment of peak have the enlarged durability for 20-30%.

Metal coats resistant to wear can be applied on the knifes of rotary cultivator, mower knifes, chopper knifes, harrow teeth, etc., with possible making of these elements of cheaper low-carbon steels.

On the larger surfaces of soil treating tools where the wear degree is different on particular segments, as is the case on the working surface of plough body, it is economical to apply hard metal coats only on the parts of surface with the highest degree of wear. This means that working surfaces of mouldboard and plowshare should be divided on segments. These segments, where the fast wear occurs occurred, should be protected with metal coats. Besides high hardness and wear resistance, metal coat should have a lower friction due to decreasing of pulling force. Appliance of metal coatings enables many advantages related to selection of basic material as well as to making and selection of different dimensions - thickness of basic materials and coats.

LITERATURE

[1.] *Ercegović, Đ.*, **New conceptions of mechanisation for soil tillage, sowing and applying of fertilisers and pesticides**, doctoral thesis, Faculty of Mechanical Engineering, Belgrade, 1987.

[2.] *Majuskas, I. S. i dr.*, **Investigation of pressure distribution on the plowshare surface during the tillage, Tractors and agricultural machines**, Moskow, 11/58.

[3.] *Novaković, Vl., Ercegović, Đ.*, **Importance of investigation of friction and wear for different types of agricultural machinery surface coats**, VI International Conference: Agricultural engineering and science 1988., Faculty of Mechanical Engineering, Belgrade, 1988.

[4.] *Severnev, M.M.*, **Wear of agricultural machinery details**, Kolos, Lenjingrad, 1972.
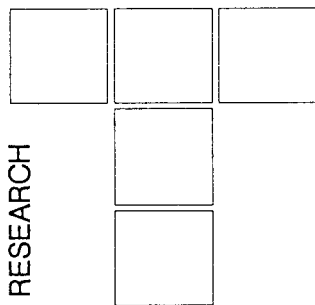
B. ROSIĆ

An Analysis of Efficiencies
of Planetary Gears

By kinematic combinations of toothed pairs with the external and internal contacts, we can obtain planetary gears with a considerably improved performance than the corresponding ones with fixed axes, as well as planetary gears with notably poor performance regarding the efficiency. In connection with this, in the reference literature and papers, it is almost regularly emphasized that planetary gears, under the same technical conditions have a smaller mass and a higher degree of efficiency than the ones with fixed axes. One of the aims of the present paper is to check the above statement and to determine the scope of the gear ratios in which the planetary gears are more suitable than the gears with fixed axes.

Keywords: planetary gear, efficiency, gear ratio, torque, central gear, satellite.

1. INTRODUCTION

Gear trains in operation are characterized by losses in the mechanical energy arising as a consequence of friction between the contact surfaces of the meshing teeth and the friction in the bearings. The power losses within the gears are expressed by means of the efficiency, and depend upon the type of gear train, the bearing, precision of manufacture, loading, lubrication, etc. With regard to the growing requirements concerning the economical consumption of energy, the efficiency represents a very significant qualitative and quantitative performance of gears. The paper considers certain variant constructions of single stage and two-stage planetary gear trains for which certain efficiencies, as well as the ranges of the practical applications of gear ratios in which planetary gears are more suitable than gears with fixed axes.

2. DETERMINATION OF INSTANTANEOUS EFFICIENCY

In most of the classical works as well as in a great number of more recent publications in which the efficiency of gearing was analyzed, some kind of average coefficient of friction representing the frictional phenomena during the gear engagement was used. In this paper, however, the coefficient of friction is treated as a variable factor during the engagement cycle. It was also assumed that the frictional losses in gearing are not only due to the relative sliding velocity of the two surfaces, but also to the combination of rolling and sliding motion of tooth surfaces.

Dr Božidar Rosić, assistant professor
Faculty of Mechanical Engineering, Belgrade

The instantaneous efficiency is determined according to the expression:

$$\eta_i = \frac{T_2}{T_1} \cdot \frac{1}{i} \qquad (1)$$

where: T_1 - external torque acting on the driving gear, Nm.
T_2 - external torque acting on the the driven gear, Nm
i - gear ratio.

The overall efficiency for gearing under consideration is determined according to:

$$\eta_a = \frac{1}{l} \cdot \int_{A_1}^{E_1} \eta_i \cdot dx \qquad (2)$$

whereby: l - active length on teeth.

In [4] is given an iterative procedure for determination of the instantaneous efficiency of a gear pair for both external and internal gearings. Based upon the models developed, computer programs for instantaneous efficiency determination were devised. The computer numerical results for determination of the instantaneous efficiency of a gear pair with internal gearing are shown in Fig.1.

The intensity of friction is determined according to:

$$F_{\mu(x)} = \mu(x) \cdot F_n \qquad (3)$$

where:

$$\mu(x) = 0.0127 \cdot log\left(\frac{\frac{29.66}{b} \cdot F_n}{\eta \cdot v_S \cdot v_R^2}\right) \text{ - coefficient of friction.}$$

where v_S - sliding velocity, m/s.
v_R - rolling velocity, m/s.
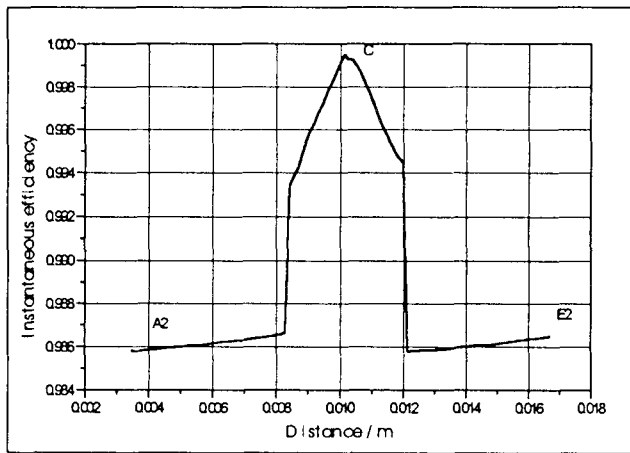η - fluid dynamic viscosity, Ns/m^2.

Fig. 1. Variations of instantaneous values of the efficiencies
for the couple under consideration during
the contact period

The intensity of the rolling friction is determined according to:

$$F_R(x) = C \cdot h(x) \cdot b \qquad (4)$$

where: b - width of gear, m.

$$h(x) = 1.6 \cdot \alpha^{0.6} \cdot (\eta \cdot V_R)^{0.7} \cdot E^{0.003} \frac{R^{0.43}}{F_n^{0.13}}$$ - the equation for minimum film thickness is due to Dowson and Higginson [1].

α - Viscosity-pressure coefficient of lubricant, m^2/N.
R - Effective radius of curvature, m.
E - Young modulus of gear material, N/m^2

On the basis of the models developed for a gear pair with external and internal gearing, the efficiency of a planetary gear train can be determined.

3. THE SINGLE STAGE PLANETARY GEAR TRAIN

Before approaching the determination of the planetary gear train efficiency, it is, first of all, necessary to identify the driving and the driven members of the planetary gear. Specifically, for the given gear, the central gear is the driving, and the satellite is the driven member. The total power through the planetary gear train is carried partly by conjugating the gear sets, and partly by coupling. The conjugating power, i.e., the relative power, is represented by the product of the torque and the relative angular velocity of the member under consideration:

$$P_{Ha} = T_a \cdot \omega_{ra} = T_a \cdot (\omega - \omega_H) \qquad (5)$$

where: T_a - torque acting on the pinion, Nm.
ω_a - Absolute angular velocity of the central gear, rad/s.
ω_{ra} - relative angular velocity
ω_H - angular velocity of the satellite carrier, rad/s.

The coupling power can be defined as the product of the torque and the angular velocity of the transmission, i.e., the angular velocity of the satellite carrier:

$$P_{sa} = T_a \cdot \omega_H \qquad (6)$$

Accordingly, the absolute power of the central gear of the planetary gear train equals to the sum of the conjugating power and the coupling power. For an analysis of the efficiency of a planetary gear train, it is necessary to know the ratio between the relative power and the absolute power of the central gear, which may be written in the following form:

$$\varphi_a = \frac{P_{Ha}}{P_a} = 1 - \frac{\omega_H}{\omega_a} = 1 - \frac{1}{U_{aH}^b} \qquad (7)$$

Fig. 2 represents the value of φ_a as function of the absolute gear ratio, which has the form of a hyperbole with the horizontal asymptote $\varphi_a = 1$.
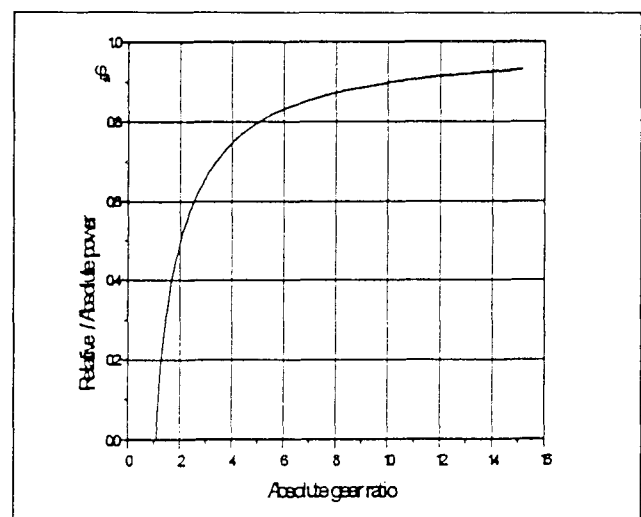

Fig.2. The ratio of the coupling and the absolute power
in the function of the absolute gear ratio

Based upon the results from Fig.2, it can be concluded that value φ_a increases with the increase of the absolute gear ratio and asymptotically approaches the real $\varphi_a = 1$. For a the total power in the gear is transferred with the conjugation of the gear sets, the same as in the gears with fixed axes. For the absolute gear ratios higher than 10, value φ_a ranges between 0.9 and 1, which means that the power is carried through the gear mainly by the conjugation of the gear sets. Thus, the practical values of the absolute gear ratios for the single stage planetary gears can be found in the range of φ_a (0.5, 0.9).

4. THE TWO-STAGE PLANETARY GEAR TRAIN

Fig. 3 represents a kinematic sketch of a two-stage planetary gear with one external and one internal contact.

The absolute efficiency for this type of gear is determined according to the following expression:

$$\eta_{aH}^{b} = \frac{1 - u_{ab}^{H} \cdot \eta_{ab}^{H}}{1 - u_{ab}^{H}} \qquad (8)$$

where: $u_{ab}^{H} = u_{ag}^{H} \cdot u_{fb}^{H} - \dfrac{z_g \cdot z_b}{z_a \cdot z_f}$ - relative gear ratio

u_{ag}^{H} - relative first stage gear ratio

u_{fb}^{H} - relative second stage gear ratio,

z_g, z_f - number of the corresponding teeth,

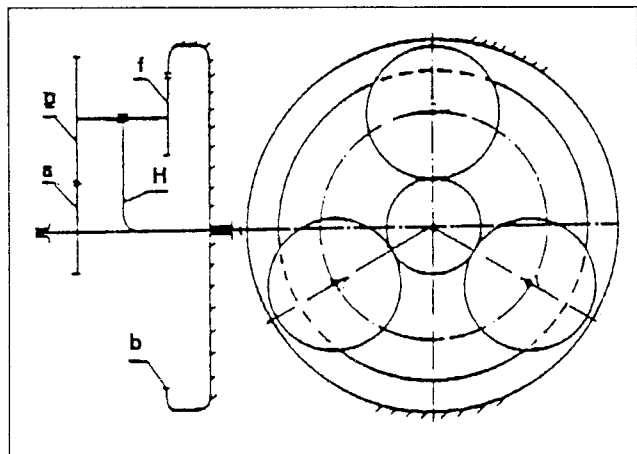$\eta_{ab}^{H} = \eta_{ag}^{H} \cdot \eta_{fb}^{B}$ - relative efficiency

Fig.3. A kinematic sketch of a two-stage planetary gear train

Commencing with the expression establishing the relationship between the absolute and the relative gear ratio:

$$u_{ab}^{H} = 1 - u_{aH}^{b} \qquad (9)$$

and after having substituted the expression for uabH in the above equation, the expression for the absolute gear ratio is obtained:

$$u_{aH}^{b} = \frac{z_a \cdot z_f + z_g \cdot b}{z_a \cdot z_f} \qquad (10)$$

The functional interdependence of the absolute efficiency upon the absolute gear ratio is shown in Fig. 4. In addition to that, the same graph shows the relative efficiency which is constant, and for the gear given, it amounts to 0.9604.

Based upon Fig. 4, it can be concluded that the absolute efficiency decreases with the increase of the gear ratio, as well as that it is higher than the efficiency of a two-stage gear with fixed axes. Keeping in mind the fact that the efficiency of the two-stage planetary gear decreases with the increase of the absolute gear ratio, it is necessary to consider the product of the efficiency and the gear ratio, which represents the relationship of the torques at the inlet and the outlet shafts of the planetary gear train (Fig.5).
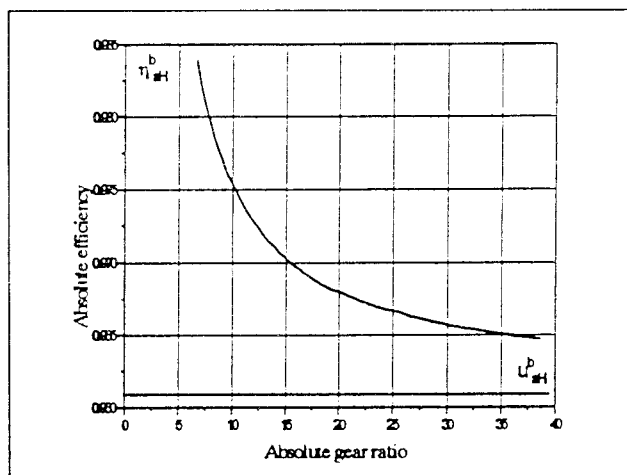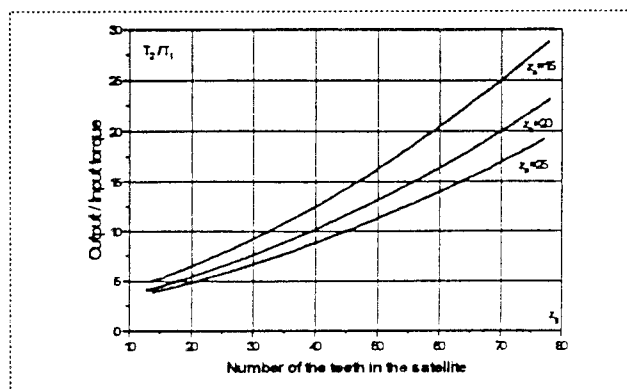

Fig. 4. The graph showing the absolute efficiency

Fig. 5. The relationship between the torques as the function of the number of the teeth

It can be seen in Fig. 5 that the relationship of the torques increases with the increase of the number of teeth in the satellite, and decreases with the increase of the number of the teeth in the central gear, so that it makes sense to apply this construction of the planetary gear train for reducing the frequency of rotation, i.e., the increase of the torque. The next construction of the two-stage planetary gear has been performed with two gears with the internal toothing. The satellite carrier, connected to the inlet shaft, the first central gear with the internal toothing is connected to the outlet shaft, while the second central gear with the internal contact is stationary (Fig. 6).
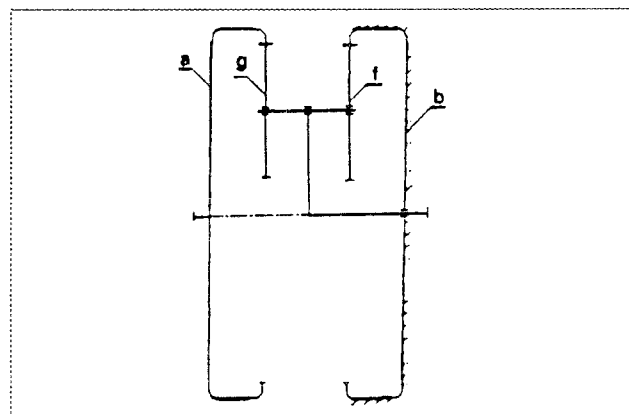

Fig. 6. A kinematic sketch of a two-stage planetary gear train

Fig. 7 and Fig. 8 show the absolute gear ratio and the efficiency of the planetary gear train as a function of the number of teeth of the satellite for definite values of the number of teeth of the central gear respectively.
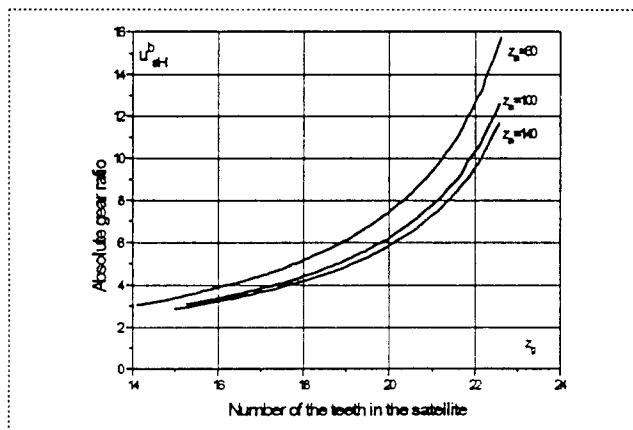

Fig. 7. The absolute gear ratio as a function of the number of teeth in the satellite
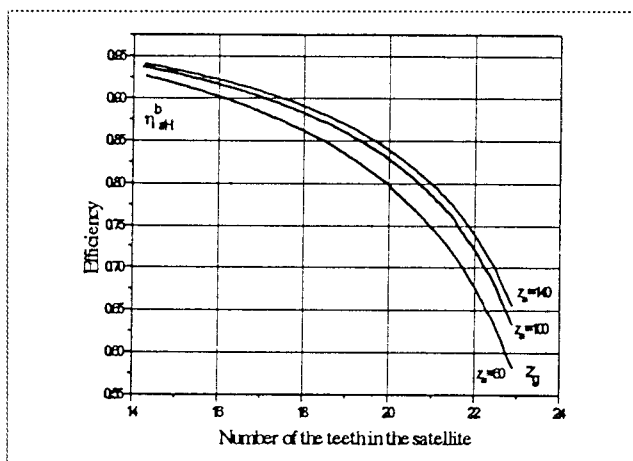

Fig. 8. The efficiency in the function of the number of teeth in the satellite

By this construction of the planetary gear relatively low values of the gear ratio, as well as of the efficiency of the gear are obtained. It should particularly be pointed out that the efficiency and the gear ratio are mutually opposite, which means that this gear also gives low values of the ratios of the corresponding torques. Therefore, it malces sense to use this type of the planetary gear only as a "kinematic" gear, i.e., for the speed transformation.

5. CONCLUSION

In accordance with the analyses described above, it can be concluded that only those types of planetary gear trains should be used that give better performance as compared to the fixed axis gear trains, and they are:

► planetary gear trains with one series of satellites - single-stage,

► the two-stage planetary gear train with one external and one internal toothing, when the central gear with the external toothing is mounted upon the inlet shaft, and the satellite carried connected to the outlet shaft at the stationary central internal gear.

REFERENCES

[1.] *DowsonD., HigginsonG.*, **Elastohydrodynamic lubrication**, S.I. Edition 1977, Pergamon Press Ltd,

[2.] *Anderson N. E., Loewenthal S. H., Black J. D.*, **An Analytical Method to predict Efficiency of Aircraft Gearboxes**, Transactions of the ASME, Vol. 108, 1986.

[3.] *Rao S. S.*, **Reliability Analysis and Design of Epycyclic Gear Trains**, ASME Journal of Mechanical Design, Vol.101, No3, 1979.

[4.] Rosić B., **Parameter Investigation and Optimisation of Planetary Gear Train Transmission**, Dsc Thesis, 1993, Mechanical Engineering Department, Belgrade University.

R. MITROVIĆ

RESEARCH

An Analysis of The Effects of The Lubricating Grease Type and The Rotational Speed Upon Operating Temperature In Sealed Roller Bearings

The working life of roller bearings is dependent on a number of factors: these include load, type and quantity of lubricant, contamination of lubricant and operating temperature. Roller bearings are usually lubricated with grease. Often they are hermetically sealed. As well as the quantity of lubricant, the type of lubricant and the rotational speed are very important factors. This paper presents an analysis of the effects of the type of lubricating grease and rotational speed on sealed roller bearings.

The research was performed under controlled conditions. The experiments were all carried out on bearings of the same type, 6204, with approximately the same degree of radial play. Testing was performed across a range of rotational speeds from 2 500 to 10 000 min^{-1}. This corresponds to a range of surface velocities $(d_s r n) = (0.08 ... 0.325) \cdot 10^6$ $mm\ min^{-1}$. For all tests, a load equivalent to 10,000 hours of life was used. The quantity of lubricant was also constant throughout the testing procedure at 20% of the free volume in the bearing. Each test was performed throughout the range of speeds until the operating temperature was stabilised, that is until thermal equilibrium was achieved within the bearing housing.

The results of this analysis will be of assistance to designers in the selection of an appropriate lubricant for bearings, depending on the rotational speed.

Keywords: Roller bearing, lubrication, type of lubricant.

1. INTRODUCTION

The reliability and working life of roller bearings depend on many different factors. One of the most common causes of failure in roller bearings is an inappropriate choice of lubricant [1]. For this reason, manufacturers of bearings pay particular attention to this problem.

More than 80% of all bearing types are grease-lubricated [4], and these are often sealed rolling bearings which require no special maintenance. In these bearings, the nominal working life is crucially dependent on efficient sealing and lubrication. Appropriate lubrication here includes the proper choice of type and quantity of lubricant for the operating conditions within the housing of the bearing.

There is little published data on the behaviour of various types of lubricating greases at different bearing speeds. Manufacturer's catalogues give only the maximum permissible rates for individual types and sizes of bearings, without reference to the type of lubricant.

Dr Radivoje Mitrovic, Junior Professor
Mechanical Engineering Faculty, University of Belgrade

This paper gives the results of comparative testing of operating temperatures for seven different types of lubricant produced by different manufacturers, identified here as A, B, C, D, E, G, and H [2].

2. TEST EQUIPMENT AND TESTING PROCEDURE

2.1 Test equipment

An apparatus for determining the limits of roling bearing rates of revolution was used for testing. A diagram of the main elements of the apparatus is shown in Figure 1.

The apparatus enables the simultaneous testing of four bearings. The loading principle is shown in Figure 2. Construction details may be found in [2] and [3].

The basic measurements were taken on type 6204 bearings from two different manufacturers. The principal data on the bearings are shown in Table 1.

The geometry of the bearings was measured precisely before assembling the components. Bearings of similar performance characteristics were chosen for testing to minimise any affect on the test results of differences in the internal geometry of the bearings.

Table 1. Principal data on bearings under test

Manufacturer	Dimensions						Load rating		Nominal speed		Material	
	d	D	B	D_k	r_1	r_2	C	C_0	n_K		rings	kage
	mm						kN		min⁻¹			
									grease	oil		
A	20	47	14	7.938	$4.1^{+0.025}$	$4.05^{+0.04}$	12.5	6.0	15000	17000	Č4146	steel
B					$4.13^{\pm0.4}$	$4.13^{\pm0.4}$	9.8	6.2	14000	18000		

A - Spindle with bearings under test and
      measuring instruments
B - Variable speed electric motor
C - Thyristor speed regulator
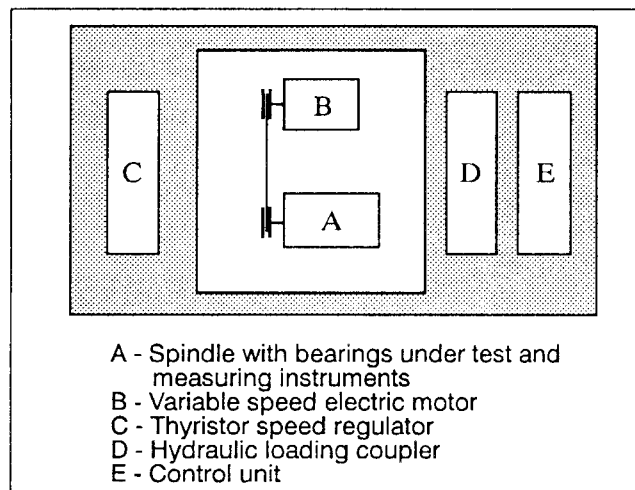D - Hydraulic loading coupler
E - Control unit

Figure 1. Layout of testing-apparatus principle components

2.2 Test Procedure

The test apparatus is preheated before the commencement of testing. The time needed for this is used to check controls and instrumentation.

All testing is carried out at a constant radial loading of $F_r = 600N$, which corresponds to the nominal life of the type 6204 bearing, *10 000 hours*. The bearing speed is changed in the course of the testing. The initial value was 0.20 n_k, where n_k is the maximum permissible speed
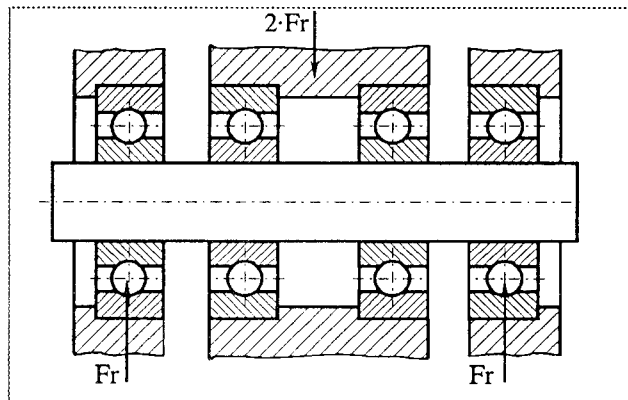

Figure 2. Diagram of loading applied to bearings under test

quoted in the manufacturer's literature. Bearing was running until thermal equilibrium reached. The speed is then increased so that the temperature increment is not excessively large. The rate of temperature changes as a function of speed for one type of lubricant is shown in Figure 3. The maximum and minimum temperatures of the sample bearings under test are given in the diagram. After each speed increment, the temperature first rises, and then falls until it stabilises. The time required to reach a stable temperature is longer at higher rates of revolution. Testing was completed when the operating temperature exceeds the temperature limit. The limit used was *100°C* upon which both the bearing and the
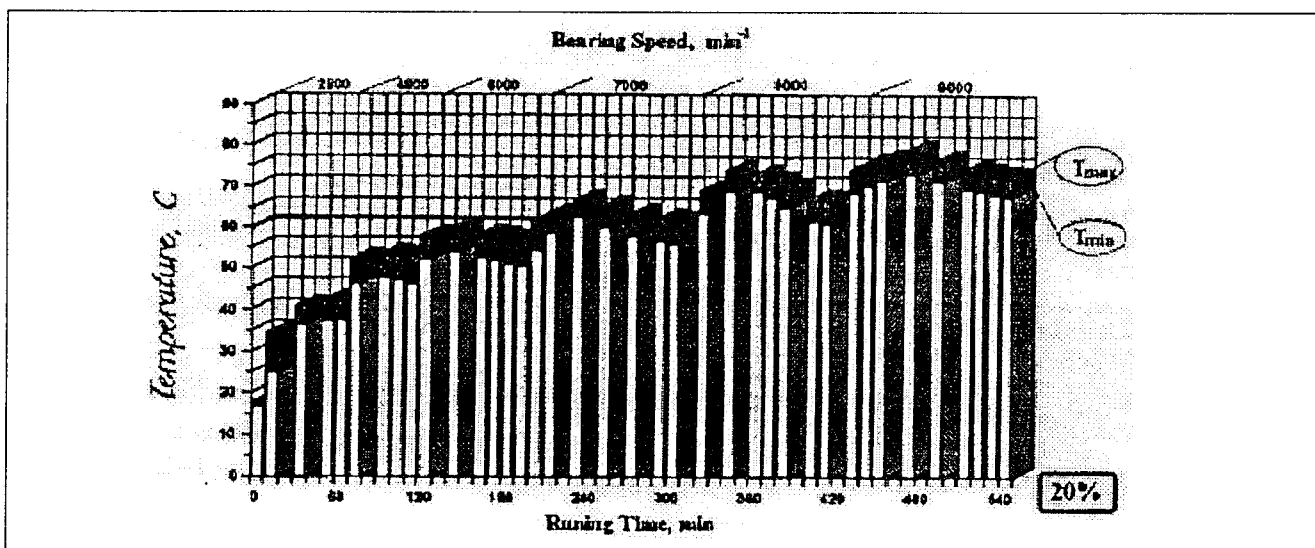

Figure 3. Changes in bearing temperature vs. bearing speed

lubricant exhibit reliable operation. Temperature, speed and load are controlled throughout the test procedure on each of the four bearings under test.

The bearings were lubricated with various types of lithium grease, with properties which meet the appropriate standards. The principal properties of these lubricants are given in Table 2.

Table 2. Principal properties of lubricants

	LUBRICANT						
	A	B	C	D	E	G	H
NGLI consistency	2	2	2	2	2	2	2
Penetration, 0.1 mm	265-295	265-295	270-290	265-295	265-295	265-295	270-290
Pour point	190	190	180	180-185	180	180185	180
Operating temperature	-35 to 125	-40 to 140	-35 to 135	-35 to 100	-30 to 110	-35 to 100	-35 to 135

3. ANALYSIS OF TEST RESULTS

3.1 Effects of the bearing internal geometry

Figure 4a shows a diagram of temperature change as a function of bearing speed for the sample of bearings using lubricant B. The ordinates show the difference between the absolute temperature of the bearing and the temperature of the environment in order to eliminate the effect of ambient temperature in the consideration of the results. The figure indicates that, with the test device being cooled only by natural convection, the lubricant can be used up to 8 000 rpm. At rates above this, the temperature of the bearing exceeds the operating limit.

Figure 4b is a diagram of temperature change as a function of bearing speed for the same sample of bearings using the same lubricant in a repeated test. It should be borne in mind that at higher speeds, part of the volume of lubricant is expelled from the working zone of the bearing. Thus the diagrams in Figure 4a and 4b are very similar but not identical.

In order to demonstrate the effects of the internal geometry of the bearings on the test results, tests were performed on the bearings of another manufacturer (B),

using the same quantity and type of lubricant. The results of these are shown in Figures 4c and 4d. Figure 4c indicates that the difference between bearings of manufacturer A and B becomes significant only at speeds over 7 000 rpm., which could be a result of a greater loss of lubricant in the working zone of the bearing, or some other incidental cause. The character of the temperature change as a function of rotational speed is almost identical in the repeated test to that recorded in the test performed on the bearings of the manufacturer A.

As the internal geometry of the bearing is determined by each manufacturer and, on this occasion, it was impossible to dismantle the bearing of manufacturer B without destroying the raceway, it was not possible to measure the geometry of the bearing elements. On the basis of these results it can be asserted that:

a) Either the internal geometry of the bearing at approximately equal values of radial play (tolerance of 1 mm) does not significantly influence the temperature of the bearing as a function of the rate of revolution, or

b) the internal geometries of the bearings produced by manufacturer A and manufacturer B are very similar, giving closely similar and analogous test results.
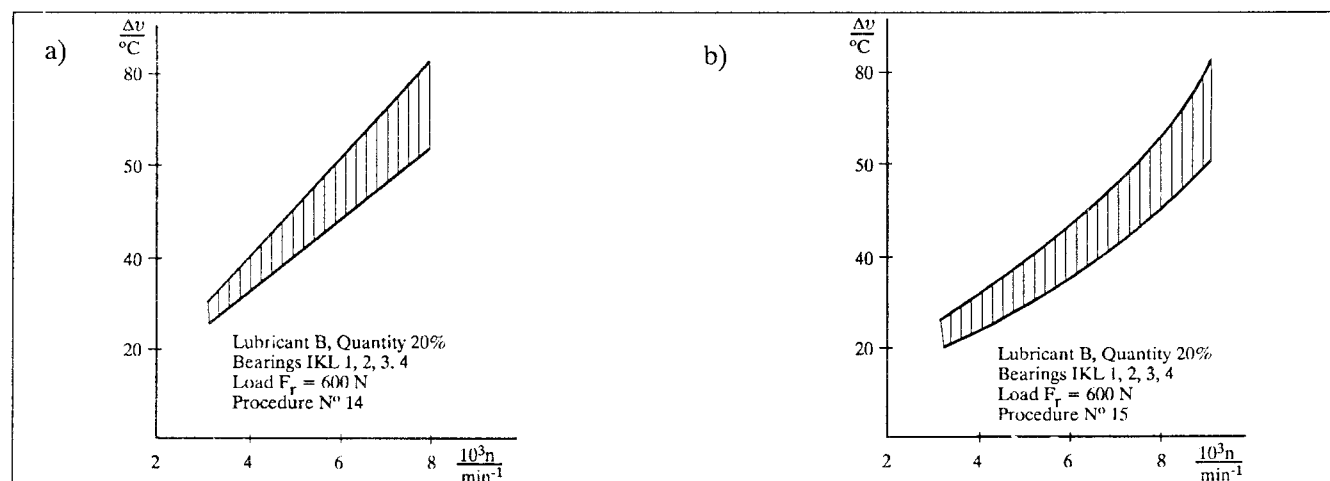
Figures 4a - 4b. Changes in bearing operating temperature vs. speed
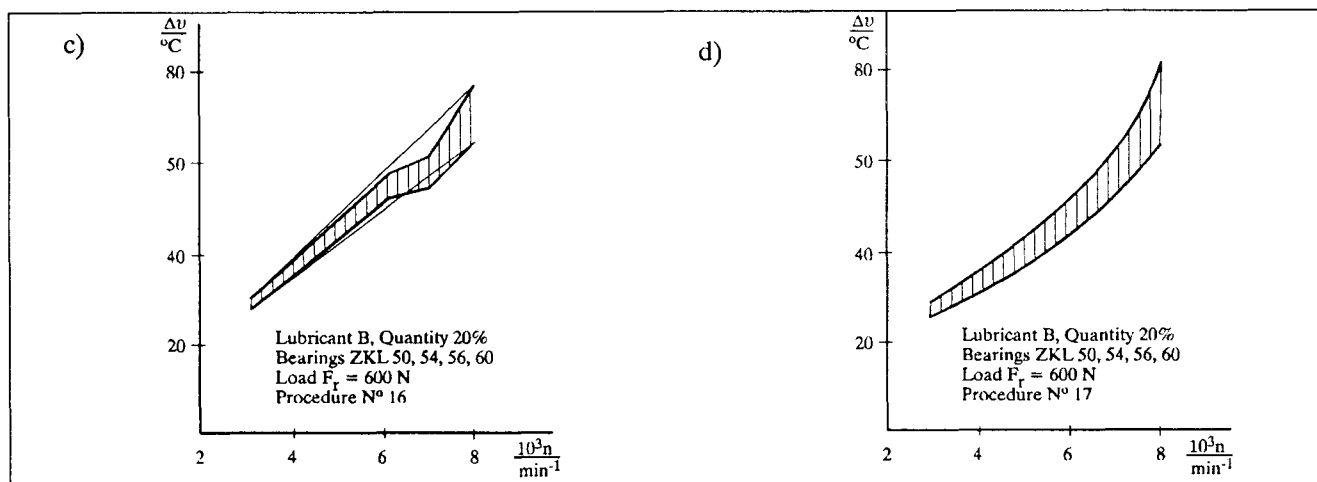
Figures 4c - 4d. Changes in bearing operating temperature vs. speed

3.2 Effect of type of lubricant

Figure 5a shows the test results for lubricant C, and Figure 5b shows the test results for lubricant D. In both cases, under given operating conditions, the lubricants could be used for speeds up to 10,000 rpm. This is approximately 25% better than the performance of lubricant B. The character of the temperature change as a function of rotational speed is similar in both cases.

Figure 5c is a diagram of temperature change as a function of bearing speed for lubricant A, which is intended primarily as an automotive lubricant. The results show that the maximum rate of revolution under test conditions was 9 000 rpm. This is a somewhat better result than that of lubricant B.

Figure 5d gives test results for lubricant E. The performance of this lubricant is significantly inferior to that of lubricants B, C and D.

The test results for lubricant G and lubricant H are given in Figures 5g and 5h respectively. According to these, lubricant G can be used at up to 9 000 rpm. Testing on lubricant H continued up to 10 000 rpm. The actual limit

of this lubricant may be even higher, as testing was discontinued at this point for technical reasons.

Based on the results given above, certain conclusions can be drawn about the relationship between the given types of lubricants and the conditions under which the bearings were tested. In order to posit a more general theory about the behaviour of various types of lubricants at various rates of revolution, it would be necessary to undertake further research along these lines. The results presented in this paper represent a basis for the consideration of these issues and for planning further experimental research.

The relationship of the mean value of the stable temperature to the dn parameter, for various types of lubricant is shown in Figure 6.

As the criterion for deciding on the choice of lubricant, this paper adopts the temperature of $80^\circ C$ because at this temperature the maximum life of the lubricant is achieved. On the basis of these test results, the designer of the bearing is able to choose the appropriate lubricant for the rate of revolution, while also taking into consideration other relevant factors for the correct and reliable work of the bearings, in other word the bearing assembly.
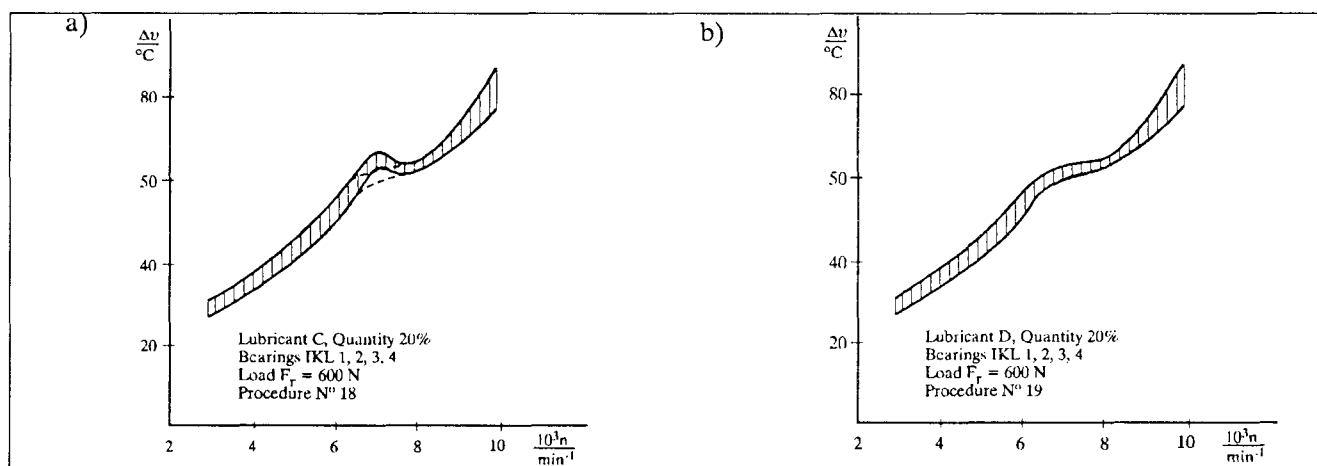
Figures 5a - 5b. Changes in the bearing operating temperature vs. speed
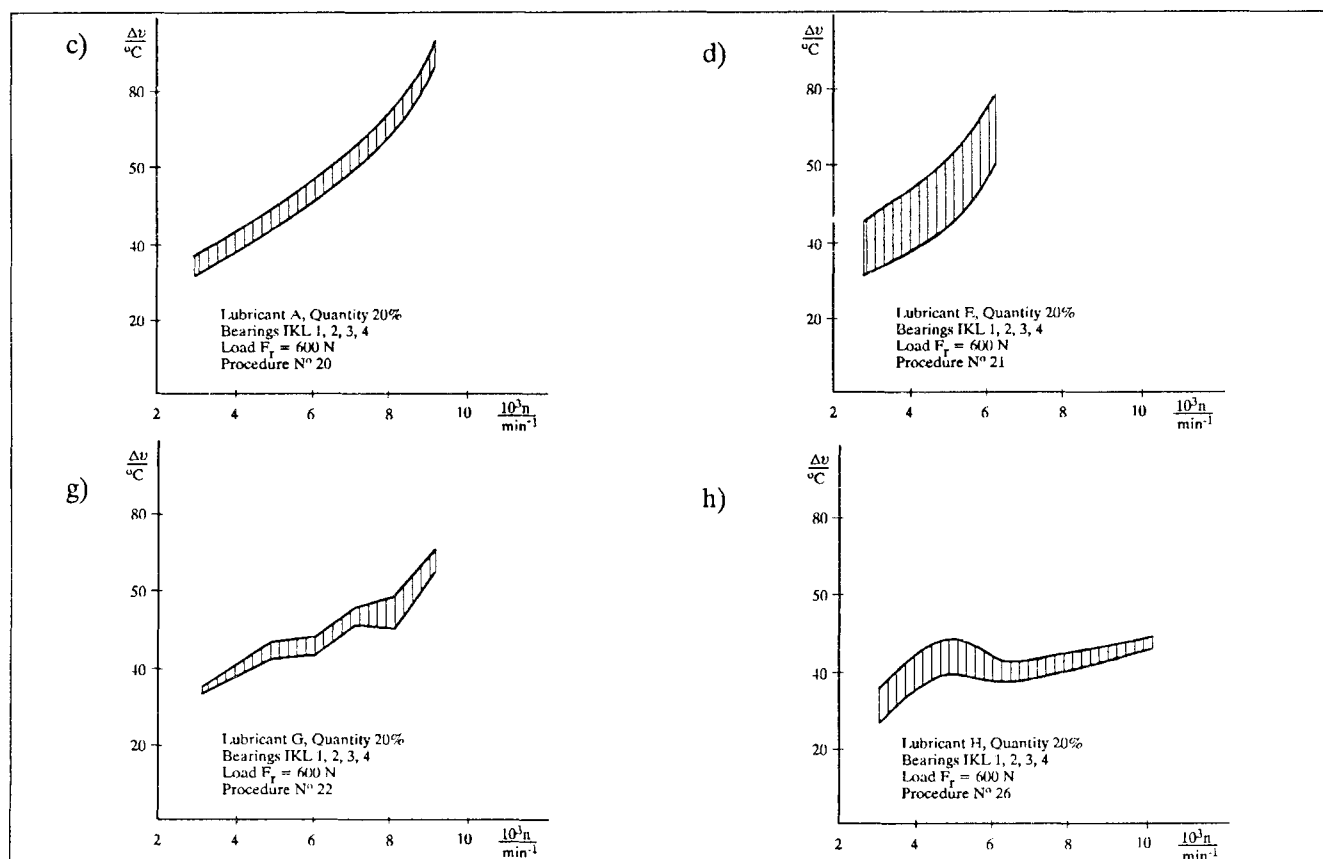
Figures 5c - 5h. Changes in the bearing operating temperature vs. speed

4 CONCLUSION

The operating temperature and the effective working life of both lubricant and bearing are greatly affected by the type of synthetic lubricant (grease) with which the bearing is packed.

The experimental research described here establishes that there is a relationship between operating temperature and rotational speed for various types of lubricants, when other parameters are approximately constant. Ba-
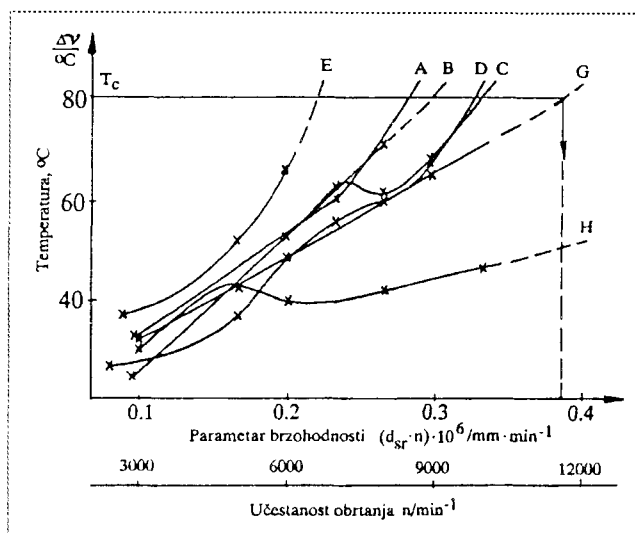

Figure 6. Bearing mean temperature vs dn parameter, for various lubricants

sed on the relationships thus established, the bearing designer is able to make an informed choice as to the type of lubricant to be used. Other factors which are important for the proper and reliable functioning of the bearing must also be taken into account.

In order to develop a general theory about the influence of various types of lubricants on the operating temperature of the bearings, in other words on the working life of the lubricant and the bearing, at various speeds, it would be necessary to consider other factors which influence this, such as quality of lubricant and loading. The results given in this paper represent a contribution to this area and a basis for further research.

BIBLIOGRAPHY

[1.] *Harris J. H.*, The Lubrication of Rolling Bearings. Published by Shell Co., London 1967.

[2.] *Mitrovic R.*, Research into the influence of design and tribological parameters of the roller bearing upon bearing function at high rates of revolution. (in Serbian). Dissertation, Univ of Belgrade 1992.

[3.] *Mitrovic R.*, Research into the influence of radial play on the rate of revolution limit for roller bearings lubricated with synthetic lubricants. (in Serbian). In: Tribology in Industry, 4, 1994.

[4.] SKF Electronic Catalog, 1996